BLANKET ENGINEERING

KEYWORDS: *integral neutronics experiments, tritium breeding, nuclear heating*

JAPAN ATOMIC ENERGY RESEARCH INSTITUTE/UNITED STATES INTEGRAL NEUTRONICS EXPERIMENTS AND ANALYSES FOR TRITIUM BREEDING, NUCLEAR HEATING, AND INDUCED RADIOACTIVITY

M. A. ABDOU *University of California, Los Angeles*
School of Engineering and Applied Science
Mechanical, Aerospace, and Nuclear Engineering Department
Los Angeles, California 90095

H. MAEKAWA and Y. OYAMA *Japan Atomic Energy Research Institute*
Department of Reactor Engineering, Tokai Research Establishment
Tokai-mura, Naka-gun, Ibaraki-ken, 319-11 Japan

M. YOUSSEF *University of California, Los Angeles*
School of Engineering and Applied Science
Mechanical, Aerospace, and Nuclear Engineering Department
Los Angeles, California 90095

Y. IKEDA *Japan Atomic Energy Research Institute*
Department of Reactor Engineering, Tokai Research Establishment
Tokai-mura, Naka-gun, Ibaraki-ken, 319-11 Japan

A. KUMAR *University of California, Los Angeles*
School of Engineering and Applied Science
Mechanical, Aerospace, and Nuclear Engineering Department
Los Angeles, California 90095

C. KONNO, F. MAEKAWA, K. KOSAKO, and T. NAKAMURA
Japan Atomic Energy Research Institute, Department of Reactor Engineering
Tokai Research Establishment, Tokai-mura, Naka-gun, Ibaraki-ken, 319-11 Japan

E. BENNETT *Argonne National Laboratory, Fusion Power Program*
Building 205, 9700 South Cass Avenue, Argonne, Illinois 60439

Received February 2, 1995
Accepted for Publication April 13, 1995

A large number of integral experiments for fusion blanket neutronics were performed using deuterium-tritium (D-T) neutrons at the Fusion Neutronics Source facility as part of a 10-yr collaborative program between the Japan Atomic Energy Research Institute and the United States. A series of experiments was conducted using blanket assemblies that contained Li_2O, beryllium, steel, and water-coolant channels with a point neutron source in a closed geometry that simulated well the neutron spectra in fusion systems. Another series of experiments was conducted using a novel approach in which the point source simulated a pseudo-line source inside a movable annular blanket test assembly, thus providing a better simulation of the angular flux distribution of the 14-MeV neutrons incident on the first wall of a tokamak system. A number of measurement

techniques were developed for tritium production, induced radioactivity, and nuclear heating. Transport calculations were performed using three-dimensional Monte Carlo and two-dimensional discrete ordinates codes and the latest nuclear data libraries in Japan and the United States. Significant differences among measurement techniques and calculation methods were found. To assure a 90% confidence level for tritium breeding calculations not to exceed measurements, designers should use a safety factor >1.1 to 1.2, depending on the calculation method. Such a safety factor may not be affordable with most candidate blanket designs. Therefore, demonstration of tritium self-sufficiency is recommended as a high priority for testing in near-term fusion facilities such as the International Thermonuclear Experimental Reactor (ITER). The radioactivity measurements were performed for >20 materials with the focus on gamma emitters with half-lives <5 yr. The ratio of the calculated-to-experimental (C/E) values ranged between 0.5 and 1.5, but it deviated greatly from unity for some materials with some cases exceeding 5 and others falling below 0.1. Most discrepancies were attributed directly to deficiencies in the activation libraries, particularly errors in cross sections for certain reactions. A microcalorimetric technique was vastly improved, and it allowed measurements of the total nuclear heating with a temperature rise as low as 1 μK/s. The C/E ratio for nuclear heating deviated from 1 by as much as 70% for some materials but by only a few percent for others.

I. INTRODUCTION

In fusion systems operated on a deuterium-tritium (D-T) cycle, 14-MeV neutrons serve two important functions: (a) producing sensible heat for energy conversion and (b) breeding tritium to close the fuel cycle. Besides these two useful functions, neutrons have many adverse effects that must be guarded against. Examples of such effects are induced radioactivity and its associated decay heat and also radiation damage to components. Thus, radiation shielding is necessary to protect components, workers, and the public.

Recent successes in burning tritium in the Joint European Torus[1] (JET) and Tokamak Fusion Test Reactor[2] (TFTR) have already necessitated the need to deal with some of the neutronics and shielding issues. Furthermore, the present engineering design activity for the International Thermonuclear Experimental Reactor (ITER) is faced with the need to address the full range of neutronics and shielding issues. The nuclear design[3] of ITER requires a comprehensive prediction capability that includes computer codes and data libraries. Verification of the prediction capability and validation of the engineering design must be accomplished primarily by conducting relevant experiments. In addition, methodologies for quantifying uncertainties and providing design safety factors become exceedingly important as the engineering design of fusion devices becomes more mature.

Almost 15 yr ago, scientists from the United States and Japan anticipated the need for experimental verification of neutronics codes and data for fusion. A new facility, called the Fusion Neutronics Source[4] (FNS) was constructed at the Japan Atomic Energy Research Institute (JAERI) to produce 14-MeV neutrons for fusion neutronics experiments. A collaborative program between the United States and Japan on fusion neutronics was planned in the early 1980s and was formalized in 1984. This formal JAERI/U.S. collaborative program continued for 10 yr. The program included conducting neutronics integral experiments as well as pre- and post-experiment analyses.

The objectives of the JAERI/U.S. collaborative program were

1. to establish new experimental techniques for fusion neutronics integral experiments
2. to develop adequate instrumentation techniques for accurate measurements of nuclear responses
3. to validate computer codes and nuclear data libraries through an elaborate methodology that involved performing integral experiments and measuring key nuclear responses, performing analyses to predict the nuclear responses using state-of-the-art codes and data libraries, comparison and analysis of measured and calculated responses and identifying sources of discrepancies, and improvements in codes and data libraries as well as experimental techniques
4. to provide quantitative estimates of uncertainties in predicting nuclear responses
5. to provide feedback to data evaluators and code developers and guidelines to nuclear designers.

More than 20 integral neutronics experiments were conducted and fully analyzed over the past decade in the course of the JAERI/U.S. collaborative program. They represent the largest investment made to date in the field of fusion neutronics. The experimental data and the comprehensive analysis of the experiments in this program represent a wealth of information for further analysis, interpretation, and utilization by researchers and designers.

A number of papers were published over the past several years (see, for example, Refs. 5 through 24) that presented results from the earlier experiments of the collaborative program. The results of the more recent

experiments and analyses will appear concurrently with this paper (Refs. 25 through 39). Each of these papers deals with the details of a specific technical area of the collaborative experiments and analyses.

The purposes of this paper are to briefly describe the key features of the experiments, summarize the important results of analysis and measurement technique development, and provide an interpretation of the impact of the main findings on fusion development. Section II is a brief summary of the neutronics issues whose purpose is to provide appreciation of the experimental and analytical approach in this work and to provide indication of further effort required in fusion neutronics research and development (R&D). Section III presents a description of the integral experiments performed in the collaborative program, including geometry, configuration, materials, measurement techniques, and calculation methods. Highlights of the experimental and analytical results and their interpretation are given in Sec. IV. A summary is given in Sec. V.

II. FUSION NEUTRONICS METHODS AND PROBLEMS

In both magnetic and inertial fusion, the neutronics field is concerned with both utilization of and protection against neutrons and secondary gamma rays. Conversion of the kinetic energy of neutrons and the energy of secondary gamma rays occurs in the in-vessel components (e.g., divertor plates in tokamaks or the wall protection system in inertial fusion) and in the first-wall/blanket system. Tritium breeding via interaction of neutrons with lithium-containing materials is accomplished in the blanket. Fusion neutronics is also concerned with calculating the nuclear responses that provide the bases for predicting radiation effects and induced radioactivity and decay heat in the in-vessel components and the first-wall/blanket system.

A fusion device must have a variety of radiation shields. The functions of the shielding systems are (a) to protect components from intolerable levels of radiation damage, nuclear heating, and induced activation and decay heat that may result in maintainability, safety, and disposal problems and (b) to protect workers as well as the general public from intolerable radiation exposure at all times during operation, shutdown, scheduled maintenance, and random failures.

To help understand the fusion neutronics issues, it is useful to briefly review the general aspects of the configuration and material options for fusion systems. This is given below for magnetic fusion energy (MFE) and inertial fusion energy (IFE) systems.

II.A. Configuration Options

Figure 1 shows a perspective view of the general features of a tokamak. The toroidal plasma has generally a D-shaped cross section and is circumscribed by

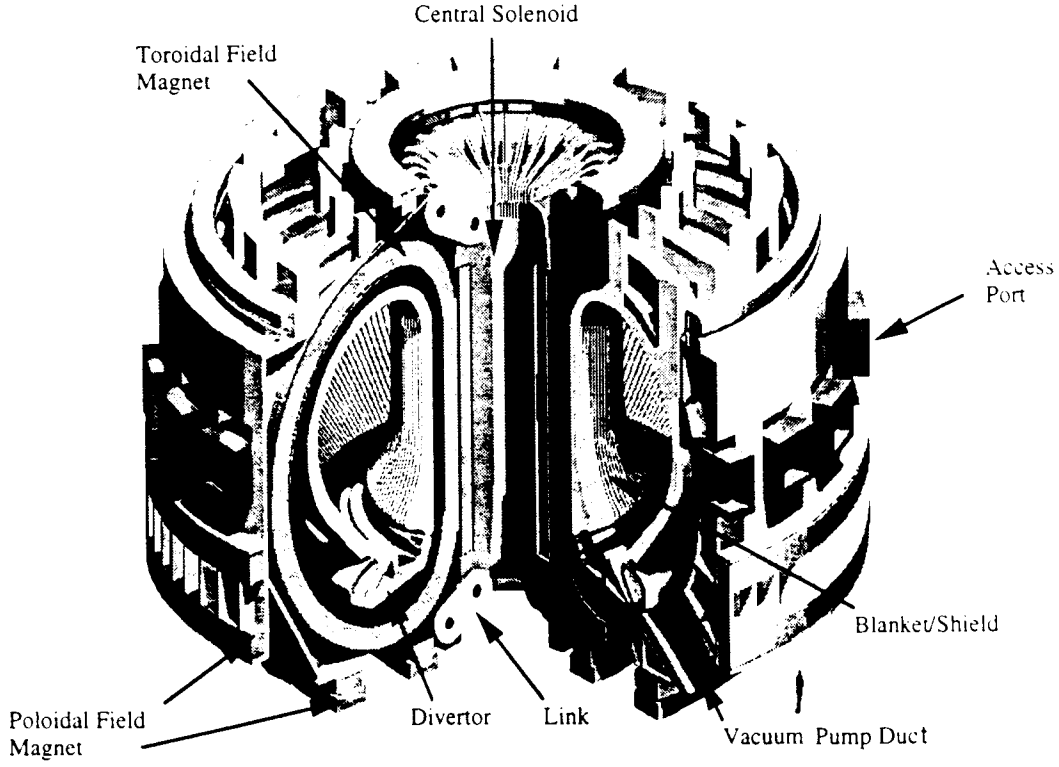

Fig. 1. Schematic isometric view of the core of a tokamak reactor.

the first wall, blanket, and bulk shield (also called primary or magnet shield). The toroidal field coils are generally superconducting,[40] but normal-conducting coils are used in present plasma devices and as possible options for fusion testing facilities. As illustrated in Fig. 1, other magnet sets exist, e.g., for ohmic heating and equilibrium field.

The complexity of the tokamak shielding is due in large part to the presence of penetrations.[41-43] These are void regions penetrating the first wall, blanket, and primary shield. The penetrations exist in a variety of sizes and shapes, and they serve critical functions for supporting and sustaining plasma operations. Examples of such penetrations are (a) divertor void regions at the bottom (and at the top in some designs) for evacuation of plasma exhaust; (b) void penetrations for auxiliary plasma heating, which are generally large in size, ~1 m^2; they are straight ducts from the first wall to the neutral beam injector in the case of neutral beams, or they may have some bends in the case of radio-frequency heating; and (c) other penetrations for fueling, diagnostics, etc. Such penetrations result in radiation streaming to components outside the primary shield. Penetration shields are necessary in the form of local shields surrounding the penetrations as they exit from the bulk shield.

If the outermost coils of a tokamak were bounded by a cylindrical envelope, then in a power reactor, the cylinder would have a radius of ~15 to 25 m and a height on the order of 20 m. The inside of this imaginary cylinder is normally called the nuclear island. This nuclear island is placed inside a reactor building, which typically is cylindrical with an ~50-m radius and a height in the range of 30 to 70 m, depending on the design. The space inside the reactor building but outside the nuclear island (see Fig. 2) is occupied by many systems, e.g., the heat transport system, beam injectors, tritium processing system, remote maintenance equipment, massive overhead cranes, etc.

The walls of the reactor building serve two functions: biological shielding and containment. The reactor building walls typically have a thickness of ~2 m,

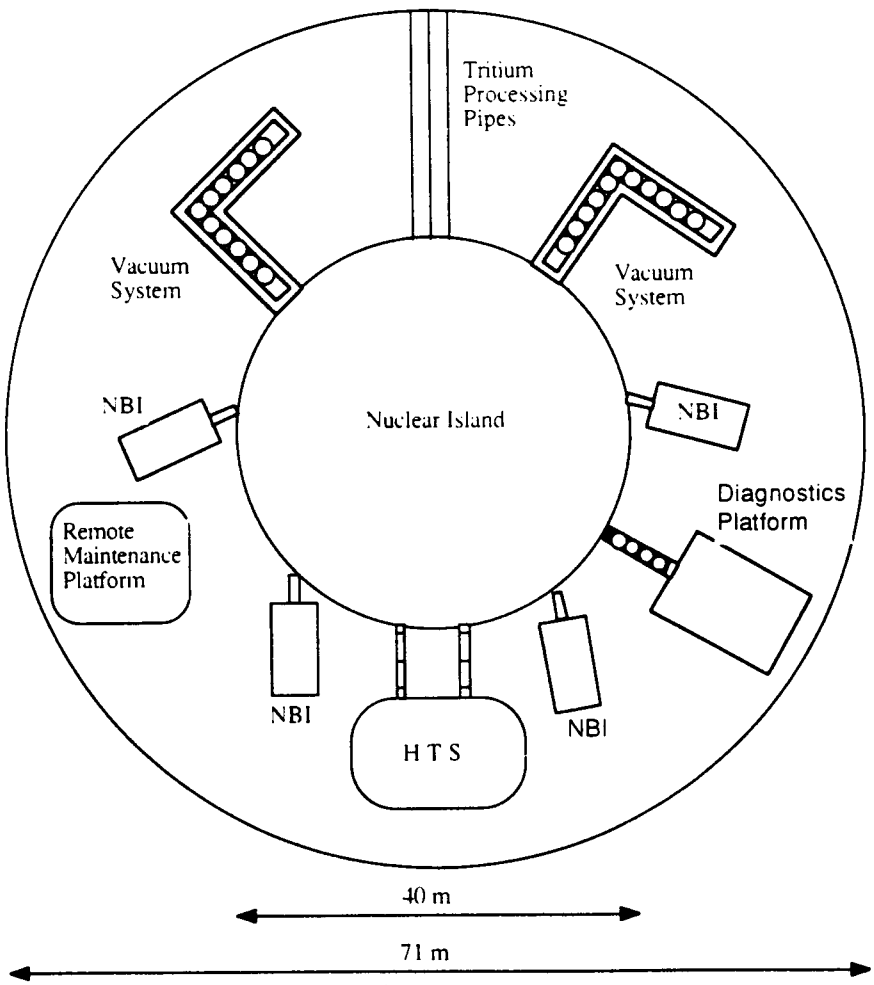

Fig. 2. Schematic representation of a magnetic fusion reactor building.

are made of special concrete, and are generally lined with a thin tritium barrier. The reactor building walls provide the biological shielding necessary to protect personnel working outside the reactor building during operation. It is impossible to allow personnel inside the reactor building during operation. Personnel access during shutdown is allowed inside the reactor building in some designs but is normally restricted to the space outside the nuclear island.[44]

The IFE systems have many common neutronics and shielding features with MFE, but they also have important differences. There are also many similarities and differences between the two mainline approaches: laser- and heavy-ion-driven systems. Figures 3 and 4 provide examples of recent IFE designs.[45] The reaction chamber in which the small D-T pellet is ignited is typically cylindrical in shape (but a spherical shape is also a possibility) with the first wall having a radius of ~5 m and a height of ~15 m. The IFE systems are pulsed with a few pulses per second. They do not have magnets or divertors. The first wall and blanket have functions generally similar to those in tokamaks, but the first wall has a protection system, e.g., a thin layer of flowing liquid metal.

An IFE power reactor generally has a bulk (primary) shield, ~1 m thick, circumscribing the blanket.

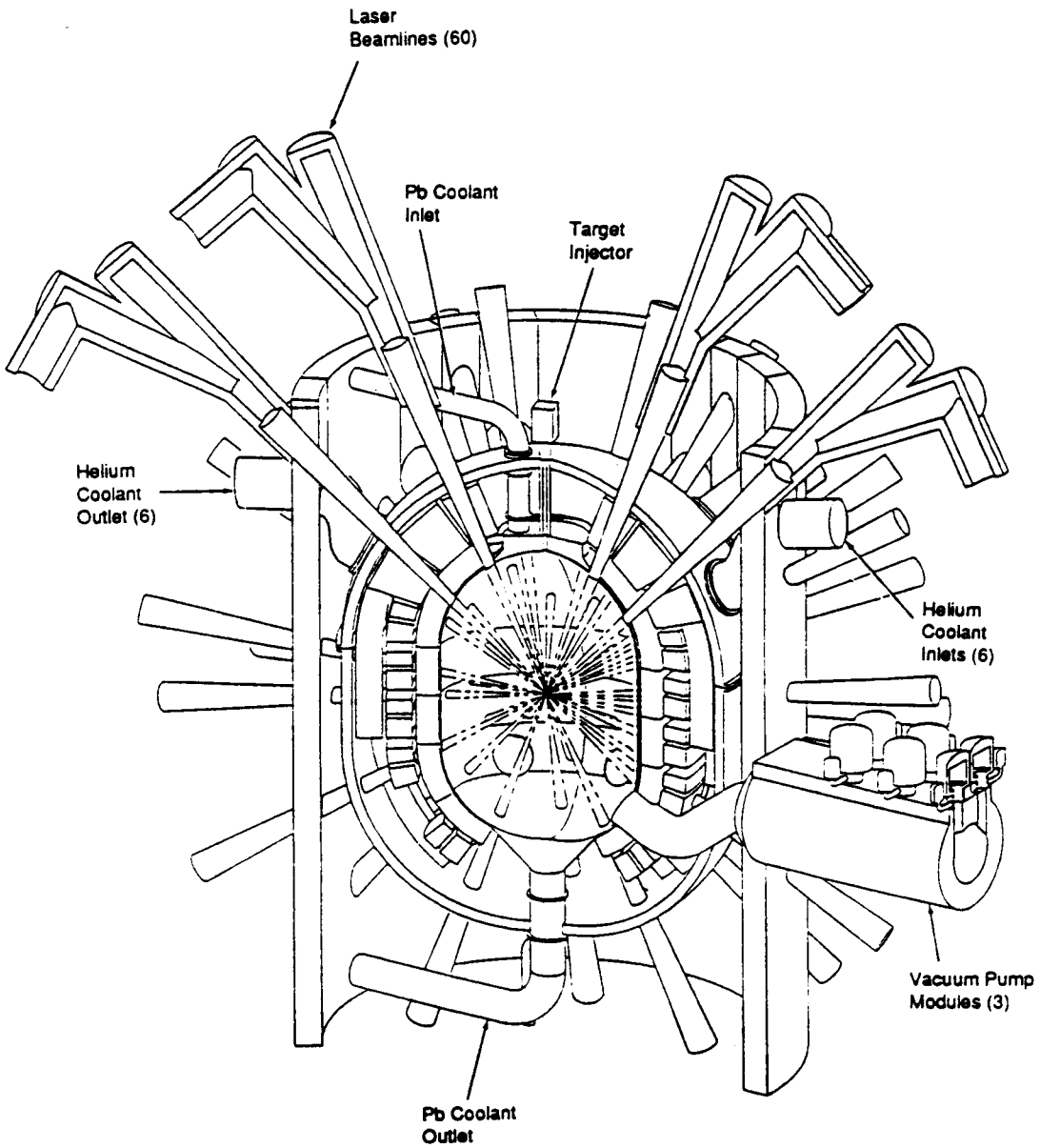

Fig. 3. Schematic view of an inertial fusion reactor with a laser driver.

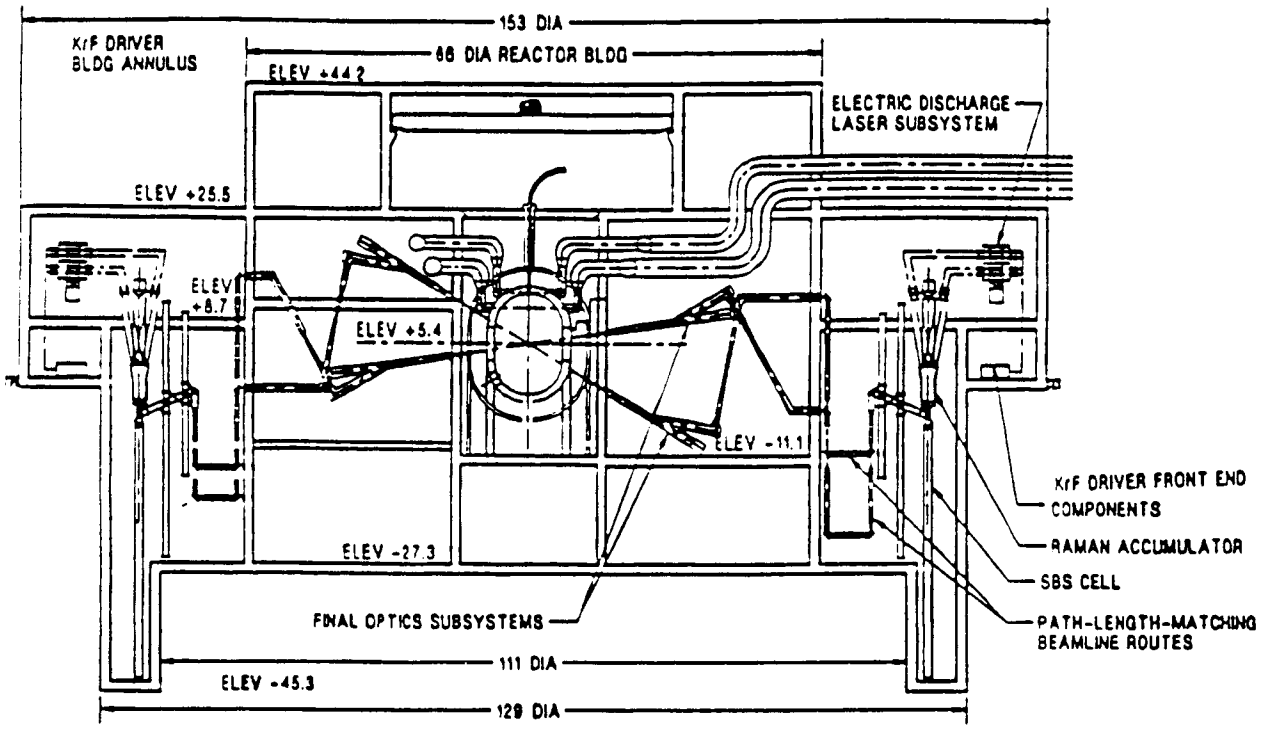

Fig. 4. Schematic view of an inertial fusion reactor building and a laser-driver building (all dimensions are in metres).

In contrast to tokamaks, where the bulk shield is designed primarily to protect the magnets, the primary shield in IFE is designed to reduce the dose and protect other components outside the cavity. Space constraints on the primary shield are much more relaxed in IFE than in tokamaks.

The IFE systems also have many void penetrations, although they are different in functions, size, and geometry from those in MFE. The dominant penetrations in IFE are those for laser or beams that supply the energy necessary to heat and ignite the D-T pellet. Typically, there are more than 40 laser beamlines but much fewer ion beamlines.

In a laser-driven fusion reactor, radiation protection of the final optics is a critical issue. Other components with important radiation protection requirements include magnets in the ion beam driver and instrumentation and control. The penetrations in IFE should be surrounded in general by local shields as they emerge from the bulk shield.

The reactor building in IFE reactors serves functions similar to those in MFE, namely, biological shielding and containment.

II.B. Material Options

The primary options for materials in the first wall and blanket are similar in IFE and MFE and are summarized in Table I. The candidate structural materials are ferritic steel, V-Ti-Cr alloys, and SiC composites. A lithium-containing material is necessary to breed tritium. The breeding material can be a solid ceramic (Li_2O, Li_2ZrO_3, Li_2TiO_3, Li_2AlO_3, or Li_4SiO_4) or a liquid (lithium or 17 Li-83 Pb). A neutron multiplier is necessary particularly with solid breeders. Beryllium is the only viable neutron multiplier with the exception of lead in LiPb.

An effective radiation shield must contain a combination of heavy, light, and neutron absorbing materials. The list of materials identified by researchers for the primary and penetration shields is limited. It includes steel, lead, H_2O, and B_4C. Tungsten has been considered for shield regions where space constraints are severe. Attempts to reduce the radioactive inventory of the massive shield led to consideration of mixtures or compounds of titanium, hydrogen, aluminum, carbon, and other low-activation materials, but no effective choice has been identified.

II.C. Nuclear Responses and Role of Integral Experiments

In fusion neutronics, one needs to perform transport calculations to predict the neutron and gamma-ray fluxes. In addition, the spatial distribution of a number of important nuclear responses must be calculated. These include

1. nuclear heating
2. tritium production

TABLE I

Worldwide Blanket Options* for DEMO

Breeder	Coolant	Structural Material
Solid breeders Li_2O, Li_4SiO_4, Li_2ZrO_3, Li_2TiO_3, Li_2AlO_3	Helium or H_2O	Ferritic steel, vanadium alloy, SiC composites
Self-cooled liquid-metal breeders Li, LiPb	Lithium, LiPb	Ferritic steel, vanadium alloy with electric insulator, SiC composites with LiPb only
Separately cooled liquid-metal breeders Lithium LiPb	Helium Helium or H_2O	Ferritic steel, vanadium alloy Ferritic steel, vanadium alloy, SiC composites

*Almost all concepts use beryllium as the neutron multiplier.

3. radiation damage indicators (e.g., helium and hydrogen productions and atomic displacements)
4. induced radioactivity
5. decay heat.

A nuclear response R, e.g., nuclear heating, tritium production, and gas production, is generally calculated from

$$R = \int_P F_R(\boldsymbol{p})\Phi(\boldsymbol{p})\,d\boldsymbol{p} \ , \tag{1}$$

where

$F_R(\boldsymbol{p})$ = response function

$\Phi(\boldsymbol{p})$ = angular flux

$\boldsymbol{p}$ = point in the phase space $(\boldsymbol{r},\boldsymbol{v})$.

In steady-state calculations, the phase space is normally represented by the spatial, energy, and angular coordinates $\boldsymbol{r}$, E, and $\boldsymbol{\Omega}$, respectively.

The neutron or photon flux is calculated by solving the Boltzman steady-state transport equation:

$$\boldsymbol{\Omega}\cdot\nabla\Phi(\boldsymbol{r},E,\boldsymbol{\Omega}) + \Sigma_t(\boldsymbol{r},E)\Phi(\boldsymbol{r},E,\boldsymbol{\Omega}) = \int d\boldsymbol{\Omega}' \int dE'\,\Sigma_s(E'\rightarrow E,\boldsymbol{\Omega}'\rightarrow\boldsymbol{\Omega})\Phi(\boldsymbol{r},E',\boldsymbol{\Omega}') + S(\boldsymbol{r},E,\boldsymbol{\Omega}) \ , \tag{2}$$

where $S(\boldsymbol{r},E,\boldsymbol{\Omega})$ is the source distribution. The neutron source distribution is normally obtained from the fusion reaction rate inside the plasma region in MFE or the target region in IFE. The source term for gamma-ray transport is obtained from photon production by neutron interactions as

$$S_\gamma(\boldsymbol{r},E_\gamma) = \sum_j N_j(\boldsymbol{r}) \int \Phi_n(\boldsymbol{r},E_n)\sigma_p^j(E_n,E_\gamma)\,dE_n \tag{3}$$

and

$$\sigma_p^j(E_n,E_\gamma) = \sum_i \sigma_i^j(E_n) f_i^j(E_n,E_\gamma) \ , \tag{4}$$

where

$\sigma_p^j(E_n,E_\gamma)$ = photon production cross section in element j

$\sigma_i^j(E_n)$ = microscopic neutron cross section in element j for gamma-producing reaction i at neutron energy E_n

$f_i^j(E_n,E_\gamma)$ = number of photons produced with energy E_γ per reaction i in element j induced by neutrons of energy E_n

N_j = nuclide density of element j.

The neutron and photon transport equations are solved using the Monte Carlo method or the deterministic discrete ordinates (S_n) method. Monte Carlo codes can model one-, two-, or three-dimensional geometric representations with continuous or discretized variables. Examples of present Monte Carlo codes are MCNP (Ref. 46), MORSE-DD (Ref. 47), GMVP (Ref. 48), and TRIPOLI (Ref. 49). The discrete ordinates codes are generally used in one, or two dimensions, but there have been recent attempts to develop discrete ordinates codes for three-dimensional geometry. Examples of present discrete ordinates codes are DOT (Ref. 50), DORT (Ref. 51), TWODANT (Ref. 52), DOT-DD (Ref. 53), and BISTRO (Ref. 54).

Neutron and photon transport calculations require extensive sets of nuclear data. Nuclear data libraries for use with transport calculations are generally processed from evaluated data files, the most common of which are ENDF/B (Ref. 55) in the United States and JENDL (Ref. 56) in Japan. Similar evaluated data files exist in Europe and the Russian Federation. Recently, the International Atomic Energy Agency started preparing the FENDL library.[57] A number of working libraries

(e.g., EFF, MATXS, etc.) are processed from the evaluated nuclear data files for use with transport codes.

The tritium production rate (TPR) at any spatial point is calculated as

$$\mathrm{TPR}(\boldsymbol{r}) = \mathrm{TPR}_6(\boldsymbol{r}) + \mathrm{TPR}_7(\boldsymbol{r}) , \quad (5)$$

where $\mathrm{TPR}_6(\boldsymbol{r})$ is the TPR from the $^6\mathrm{Li}(n,\alpha)t$ reaction with the microscopic cross section σ_6 and TPR_7 is the TPR from the $^7\mathrm{Li}(n;n'\alpha)t$ reaction with the microscopic cross section σ_7. These production rates are calculated as follows:

$$\mathrm{TPR}_6(\boldsymbol{r}) = N_6(\boldsymbol{r}) \int \sigma_6(E)\Phi_n(\boldsymbol{r},E)\,dE \quad (6)$$

and

$$\mathrm{TPR}_7(\boldsymbol{r}) = N_7(\boldsymbol{r}) \int \sigma_7(E)\Phi_n(\boldsymbol{r},E)\,dE , \quad (7)$$

where N_6 and N_7 are the nuclide densities for ^{6}Li and ^{7}Li, respectively. In this work, the quantities T_6 and T_7 are often used, where $T_6 = \mathrm{TPR}_6/N_6$ and $T_7 = \mathrm{TPR}_7/N_7$ with the neutron flux normalized to one source neutron. The tritium breeding ratio (TBR) in a reactor system is defined as the total tritium production per D-T source neutron and is calculated from

$$\mathrm{TBR} = \mathrm{TBR}_6 + \mathrm{TBR}_7 , \quad (8)$$

$$\mathrm{TBR}_6 = \int \mathrm{TPR}_6(\boldsymbol{r})\,d\boldsymbol{r} , \quad (9)$$

and

$$\mathrm{TBR}_7 = \int \mathrm{TPR}_7(\boldsymbol{r})\,d\boldsymbol{r} . \quad (10)$$

Note that in calculating TBR_6, TBR-, and TBR in Eqs. (8), (9), and (10), the neutron flux must be normalized to one source neutron. The accuracy of tritium breeding calculations depends directly on σ_6, σ_7, and the neutron flux Φ. The microscopic cross section for the $^6\mathrm{Li}(n,\alpha)t$ reaction has a relatively small uncertainty, but σ_7 has a larger uncertainty. There are additional errors in σ_6 and σ_7, as they are used in libraries for transport codes, due to inaccuracies of processing, representation, and spectrum averaging. Errors in calculating the neutron flux can potentially be large because of approximations or uncertainties in neutron source representation; approximations in modeling of geometrical shapes, heterogeneity of materials, void penetrations, etc.; approximations in the transport codes; and uncertainties in nuclear data libraries used with the transport codes, which could originate from errors and approximations in the measured differential data, data evaluation and representation of data, and data processing.

Neutronics integral experiments provide a powerful tool in providing direct measurements of the total TPR and comparing it directly to calculations. However, to identify sources of errors, integral experiments should proceed from a simple geometry with a single material to more complex geometries with multiple materials. The simpler experiments permit identification of the sources of errors and are thus more useful in providing feedback on areas of improvement to nuclear data measurements and evaluation and to code development. In the more complex experiments, it is more difficult to isolate the sources of errors, and their value tends to be more in the direction of providing designers with quantitative safety factors.

The nuclear heating rate H is obtained[58,59] by summing the neutron heating rate H_n and gamma heating rate H_γ, which are calculated from the neutron and gamma fluxes and kerma factors as

$$H(\boldsymbol{r}) = H_n(\boldsymbol{r}) + H_\gamma(\boldsymbol{r}) , \quad (11)$$

$$H_n(\boldsymbol{r}) = \sum_j N_j(\boldsymbol{r}) \int \Phi_n(\boldsymbol{r},E)k_{nj}(E)\,dE , \quad (12)$$

and

$$H_\gamma(\boldsymbol{r}) = \sum_j N_j(\boldsymbol{r}) \int \Phi_\gamma(\boldsymbol{r},E)k_{\gamma j}(E)\,dE , \quad (13)$$

where

$k_{nj}(E)$ = neutron kerma factor at neutron energy E for element j

$k_{\gamma j}(E)$ = gamma kerma factor at gamma energy E for element j.

The accuracy of nuclear heating calculations depends on the accuracy of Φ_n, Φ_γ, k_n, and k_γ. The sources of errors in Φ_n are as described earlier. The problems in calculating Φ_γ are generally similar to those with Φ_n except that the gamma-ray interaction cross sections are generally better known than those of the neutron interaction cross sections and the source term [Eq. (3)] for the gamma-transport calculation tends to be a major source of error because the gamma-ray production cross sections [Eq. (4)] currently suffer from large inaccuracies for many materials.

The gamma kerma factor k_γ is generally calculated from analytic expressions for photoelectric, pair production, and Compton-scattering processes. The neutron kerma factor k_n is more complex and is calculated from neutron interaction kinematics using specialized codes. Neutron kerma factor calculations require much more detailed nuclear data information than those needed in transport calculations. Hence, uncertainties in neutron kerma factors could be a large contributor to errors in nuclear heating calculations. This is particularly true in lighter elements where neutron heating is much larger than the gamma heating.

Prior to the collaborative program, no experiment had been performed to measure the total nuclear heating with D-T source neutrons despite the fact that the theory and calculation methods were developed[58,59]

two decades ago. In this program, the first such experiments have been performed. However, as will be discussed later, there are difficulties in conducting such experiments, particularly with respect to the required yield of the neutron source and the feasibility of separating the neutron and gamma heating components.

The key part of radioactivity calculations is to determine the nuclide densities of various radioisotopes. These are obtained from solving a coupled set of first-order differential equations:

$$\frac{dN_i(\boldsymbol{r},t)}{dt} = \sum_j N_j(\boldsymbol{r},t)\int \Phi(\boldsymbol{r},E,t)\sigma_{j\to i}(E)\,dE + \sum_k \lambda_{k\to i}N_k(\boldsymbol{r},t) - N_i(\boldsymbol{r},t) \times \sum_{b\neq i}\int \Phi(\boldsymbol{r},E,t)\sigma_{i\to b}(E)\,dE - N_i(\boldsymbol{r},t)\sum_m \lambda_{i\to m}\ , \qquad (14)$$

where

$N_i(\boldsymbol{r},t)$ = number density of nuclide i at position $\boldsymbol{r}$ at time t

$\sigma_{x\to y}(E)$ = neutron reaction cross section for transmutation of nuclide x into nuclide y by neutrons of energy E

$\lambda_{w\to z}$ = decay constant (multiplied by branching ratio, if any,) for nuclide w spontaneously decaying into nuclide z.

The radioactivity for any radioisotope i at time t is determined from $\lambda_i N_i$ once all nuclide densities at all time points of interest are calculated. The decay heat at any time t consists of two parts: The first is a term that accounts for charged particles (primarily from beta decay) produced by the decay and deposited locally, and the second is from the absorption of decay gamma rays. Normally, a decay gamma source term is calculated and used to solve the transport equation to obtain decay gamma fluxes, which in turn are used together with gamma kerma factors to calculate decay gamma heating.

The accuracy of radioactivity calculations depends on the accuracy of neutron flux, transmutation cross sections, decay constants (including branching ratios), and the radioactivity code, whose main function is to solve for nuclide densities. It has been established[60] recently that the error due to algorithms and computation of most radioactivity codes is small. The errors due to the neutron flux are as we discussed earlier, but there could be additional errors due to the assumption normally invoked that the neutron flux is not significantly affected by nuclide transmutation. Key sources of error in radioactivity calculations, as shown later, come from the transmutation cross sections and decay gamma-ray branching ratios.

Notice that radioactivity calculations require very extensive data on reaction cross sections for many nuclides, which are generally much less known than neutron transport cross sections. Obtaining accurate differential data on transmutations of isotopes is very costly and time consuming and is often not feasible. Therefore, integral neutronics experiments in which the radioactivity is measured directly in fusion-like spectra are very valuable and cost effective in validating the data.

The integral neutronics experiments described here address tritium production, total nuclear heating, and neutron-induced radioactivity. The key problem of radiation shielding was not addressed directly under the collaborative program. The primary issue in radiation shielding is the transport calculations for predicting the neutron and photon fluxes, particularly for the deep radiation penetration problems with complex geometries, in fusion systems. However, in radiation shielding design, one also needs to calculate nuclear responses such as nuclear heating and radioactivity. Therefore, the neutronics integral experiments in the collaborative program also provide valuable data to radiation shielding design.

III. DESCRIPTION OF THE INTEGRAL EXPERIMENTS IN PHASES-I, -II, AND -III

The JAERI/U.S. collaborative program on blanket neutronics started formally in 1984 and continued for 10 yr. The program involved numerous integral experiments and analyses. The primary participants were the FNS group at JAERI and the neutronics group at the University of California, Los Angeles (UCLA). Other organizations involved in the collaboration from the United States included Argonne National Laboratory, Oak Ridge National Laboratory, and Los Alamos National Laboratory. The primary facility used for the integral neutronics experiments was the FNS at JAERI.

Three general classes of integral experiments were conducted consecutively during the 10-yr period. They are referred to as Phases-I, -II, and -III. These experiments are described in this section. The description includes the neutron source characteristics and the materials, geometry, configuration, and measurement techniques in the various experiments. Calculational methods used in the analysis are also described.

III.A. Neutron Source and Facility

The neutron source[26] is based on the $^3H(d,n)^4He$ reaction using an accelerated deuteron beam and tritiated metal target system. For most experiments, a rotating target, which is water cooled, was used. The target disk rotates at 800 rpm, and the head moves up and down to change the irradiated zone of the tritiated target. The deuteron beam energy and the current at the

source are 350 keV and 20 mA, respectively. The neutron yield is 3×10^{12} n/s at the initial condition of the tritiated target.

Accurate characterization of the energy and the angular distribution of the emitted neutrons is very important for the analysis of the experiments. Substantial effort was devoted at the beginning of each series of experiments to neutron source characterization.[25] The neutron source yield is absolutely determined by the associated alpha-particle counting technique. The accuracy of this monitor is estimated to be ~2%. In the case of heavy irradiation with more than 1-mA beam, ^{238}U and ^{232}Th fission counters were used as the external neutron monitors, and they were calibrated by the associated alpha-particle counting method at a low-flux level.

The energy and angular neutron distributions were derived from detailed Monte Carlo calculations and were confirmed by experimental information, e.g., the high-energy part of the neutron spectrum and the reaction rate distributions. These calculated source distributions agree with the experiments for fast neutrons to within ~4 to 5%.

For the Phase-III experiments to be described later, where a line source was simulated, a fixed tritiated target (in target room 1) was used. This stationary target produced a neutron yield of $\sim 3 \times 10^{11}$ n/s, which is lower than that of the rotating target used in Phases-I and -II.

III.B. Geometry and Configuration of Experiments

The three phases of the experiments had substantially different geometries and configurations of the test assemblies relative to the neutron source. Phase-I was an open geometry,[5,6] Phase-II was a closed geometry,[31,32] and Phase-III had a line source arrangement.[34-37] In each phase, a series of experiments was conducted with different material configurations inside the test assembly. The experimental setup is described briefly below for each phase.

III.B.1. Phase-I Experiments

The first series of experiments in the collaborative program is referred to as Phase-I, which is characterized by an open geometry. Figure 5 shows the overall

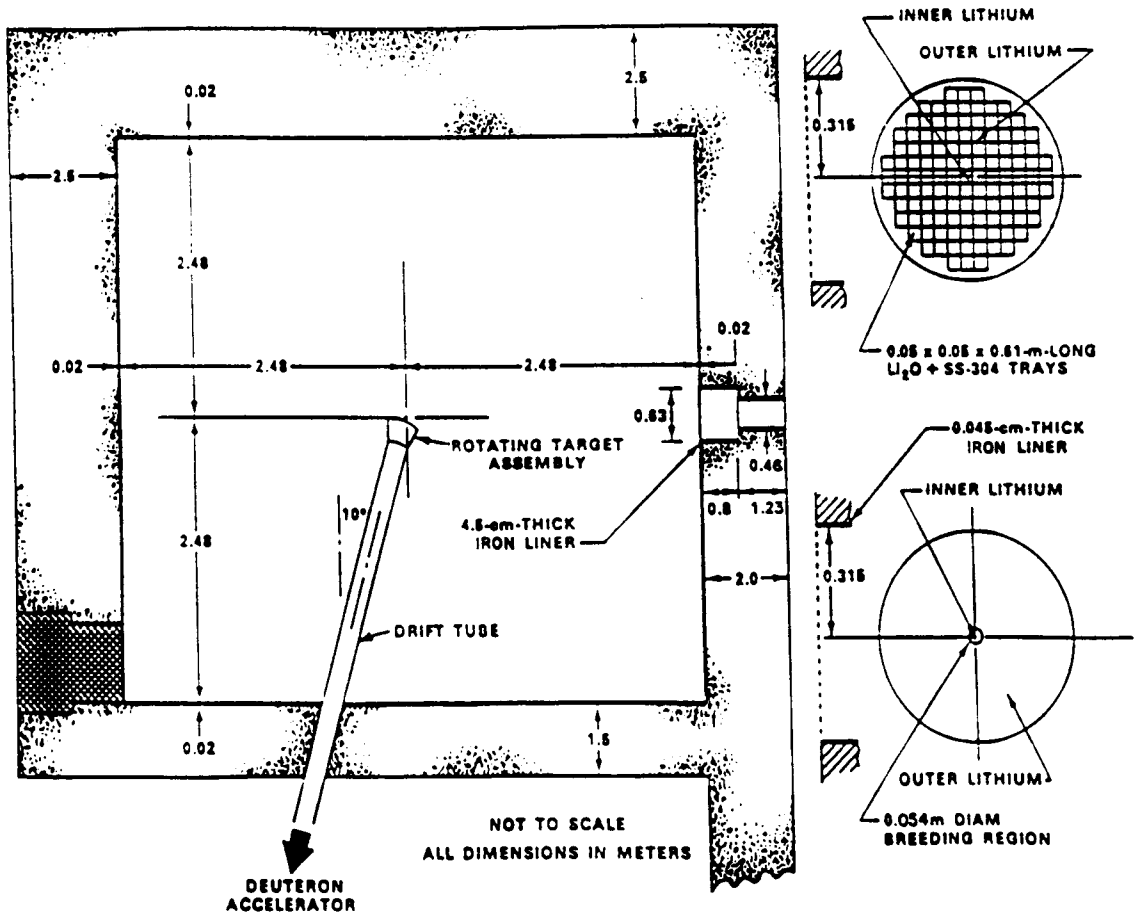

Fig. 5. Layout of Phase-I experiment.

layout of the source and the test assembly in Phase-I. The rotating neutron target (RNT) was used and was located at the center of the so-called second target room, which is 4.96 × 4.96 × 4.5 m high. The test module, which simulated a portion of a fusion blanket, was placed in an experimental port located between the two target rooms.

The basic idea of Phase-I was that the second target room represented the plasma chamber of a fusion reactor and the concrete enclosure represented the blanket region surrounding the plasma. A portion of the concrete is replaced by a breeding blanket test module, which was the focus of the experiment.

Three types of test modules were assembled in the Phase-I series of experiments,[5,6] as shown in Fig. 6: (a) the reference experiment (P1-REF), where the test assembly consisted only of the breeding material Li_2O; (b) the first-wall experiments (P1-WFW), where a 0.5-cm-thick stainless steel first wall was placed in front of the Li_2O assembly and then a 0.5-cm-thick polyethylene plate was placed between the first wall and the Li_2O (these experiments were also repeated using a 1.5-cm-thick first wall); and (c) beryllium experiments (P1-WBE), where three configurations were assembled, namely, 5-cm-thick beryllium in front of the Li_2O, 10-cm-thick beryllium in front of the Li_2O, and 5-cm-thick beryllium sandwiched between 5 cm Li_2O in front of the region and the rest of the Li_2O assembly.

III.B.2. Phase-II Experiments

As discussed later, results from Phase-I showed that it was very difficult to accurately predict the portion of the neutron flux at the front of the test assembly originating from the neutrons scattering off the concrete walls of the target room. Therefore, new experimental arrangements were developed in Phase-II to eliminate the effect of room-returned neutrons. The overall experimental layout for Phase-II is shown in Fig. 7. For the enclosure material, Li_2CO_3 was chosen to reduce cost. The breeding material in the test module remained as Li_2O. The Li_2O test module was rectangular in shape, with dimensions of 0.864 × 0.864 × 0.607 m, and constructed from Li_2O blocks. Each block consisted of cold-pressed Li_2O canned in a stainless steel box that was 0.2 mm thick. The neutron source (the target) located inside the enclosure was 0.78 m from the square front surface of the test assembly (see Fig. 7). The interior dimensions of the enclosure were 0.87 × 0.87 × 1.24 m. The Li_2CO_3 in the enclosure was 0.205 m thick with a 5-cm-thick polyethylene layer on the outside for better insulation of the room-returned neutrons. The closed geometry of Phase-II provided a good simulation of the neutron source spectrum inside the plasma chamber.

The series of experiments conducted in Phase-II consisted of three sets: IIA, IIB, and IIC. In Phase-IIA, three experiments were conducted, as shown in Fig. 8:

1. reference (P2A-REF), where the test assembly consisted only of the Li_2O breeding material
2. beryllium front (P2A-BEF), where a 5-cm beryllium slab was added in the front of the Li_2O
3. beryllium sandwich (P2A-BES), where the 5-cm beryllium region was placed in between a 5-cm Li_2O front region and the Li_2O assembly.

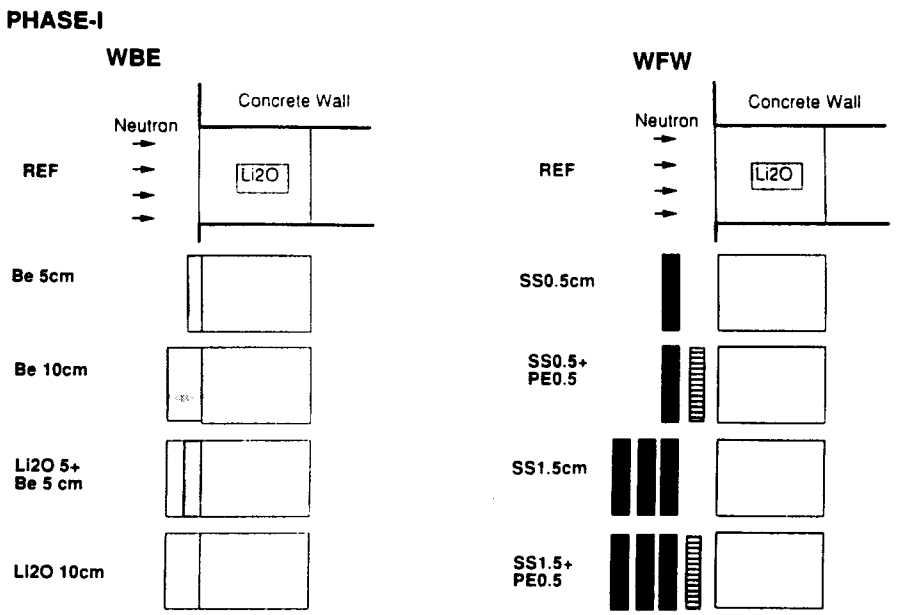

Fig. 6. Schematic of configurations for Phase-I experiments.

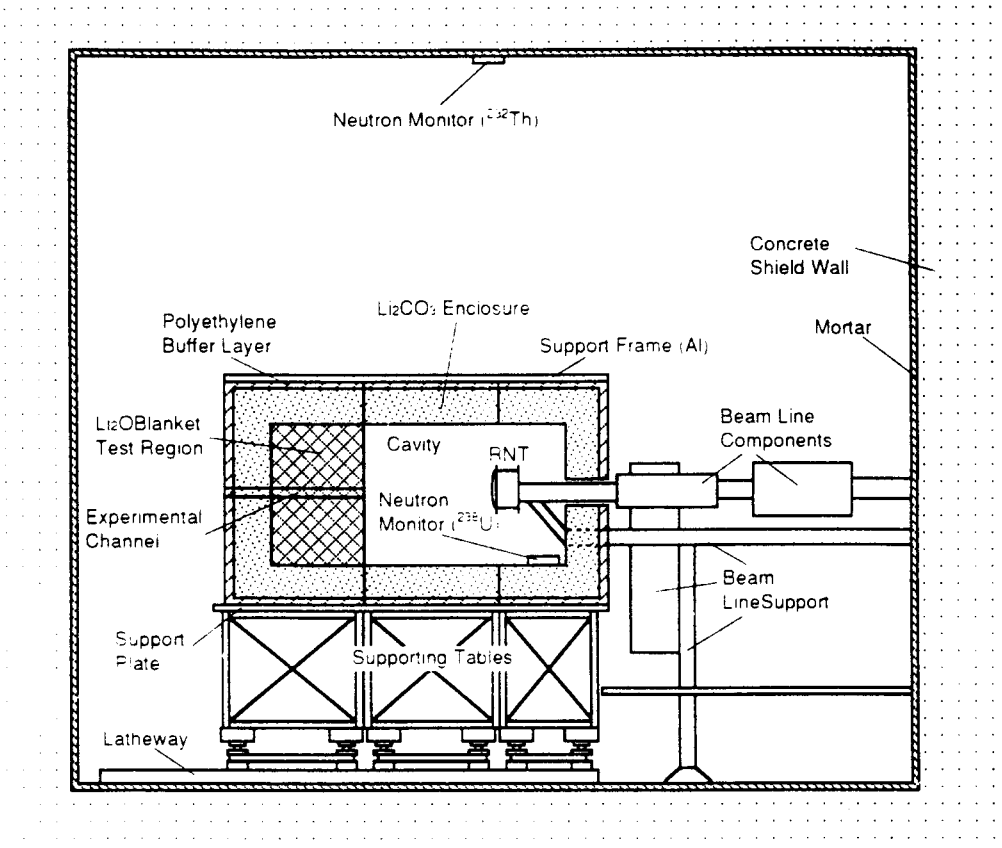

Fig. 7. Overall arrangement for Phase-II experiments.

The experiments performed in Phase-IIB were generally similar to those in Phase-IIA (Refs. 7, 8, 9, 19, and 20) except for one major difference. In all the Phase-IIB experiments, the inside surfaces of the Li_2CO_3 enclosure were covered by a 5-cm-thick beryllium layer and a 0.5-cm-thick Type 304 stainless steel first wall, as shown in Fig. 9. Three experiments were also conducted in Phase-IIB, with three different configurations for the blanket test module. In the first experiment (P2B-REF), only the Li_2O test module was used, i.e., similar to the test module in the P2A-REF experiment. In the second experiment (P2B-BEF), a 5-cm-thick beryllium region was added in front of the Li_2O blanket test module, i.e., similar to the test module in the P2A-BEF experiment. In the third experiment (P2B-BEFWFW), the blanket test assembly consisted of 0.5 cm steel first wall, followed by 5 cm beryllium and the Li_2O breeding region. Notice that the first wall and the beryllium regions in this third experiment are uniform on the inside surface of the Li_2CO_3 and the front of the Li_2O blanket test module.

Adding beryllium to the inner surface of the enclosure in Phase-IIB allowed better simulation of the softer neutron spectra inside the plasma chamber of a fusion reactor in which beryllium is used as a neutron multiplier in the blanket. This also allowed better experimental testing of the nuclear data for beryllium.

The success of the Phase-IIA and -IIB experiments led to considerations of more prototypical fusion blanket configurations in the blanket test module. Phase-IIC was then conducted to examine the effects of heterogeneity on the neutronics performance of blankets.[31-33] Two experiments were performed in Phase-IIC. The heterogeneity effects of water-coolant channels (WCCs) were examined in the first experiment (P2C-WCC), with the assembly and dimensions shown in Fig. 10. Water was simulated by polyethylene. One coolant channel was placed inside the first-wall region, and two other channels were placed at depths of 10 and 20 cm inside the blanket test region, as illustrated in Fig. 10. In the second experiment of Phase-IIC, an interesting geometrical arrangement of the beryllium neutron multiplier was examined in the so-called beryllium edge-on experiment (P2C-BEO), which is illustrated in Fig. 11. In this experiment, alternating layers of Li_2O and beryllium were arranged horizontally (rather than the normal vertical placement of the beryllium multiplier) for a depth of 30 cm followed by the Li_2O breeding region. In the

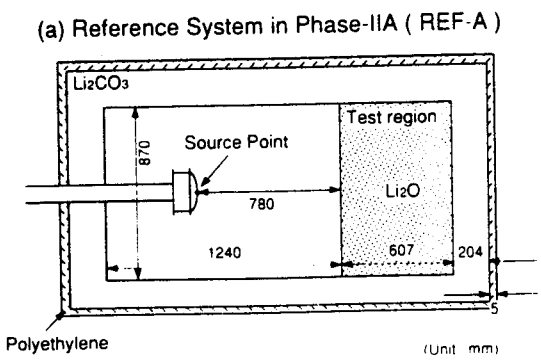

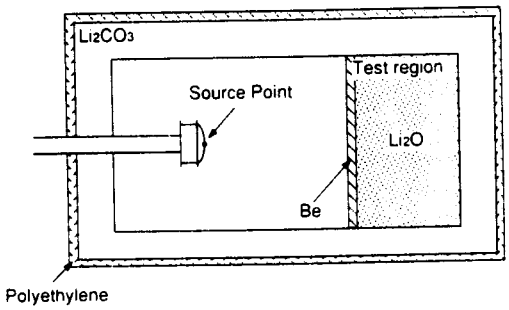

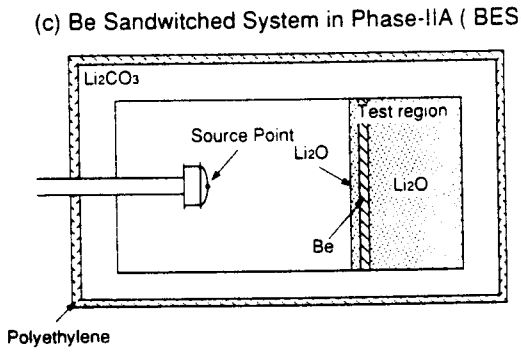

Fig. 8. Experimental arrangement for Phase-IIA.

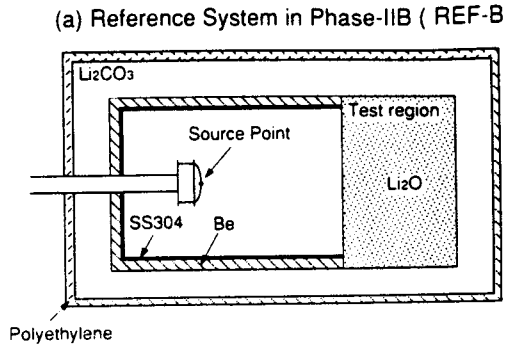

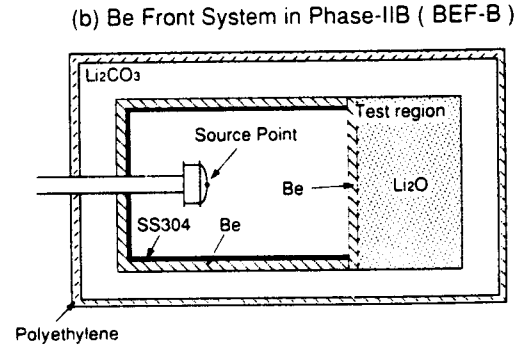

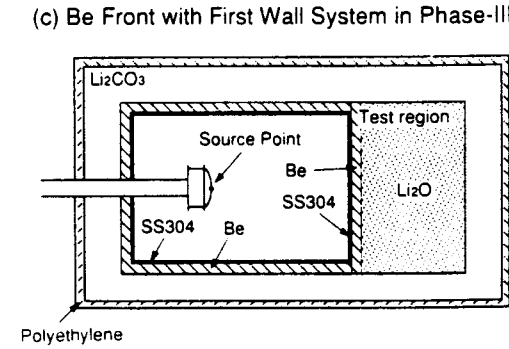

Fig. 9. Experimental arrangement for Phase-IIB.

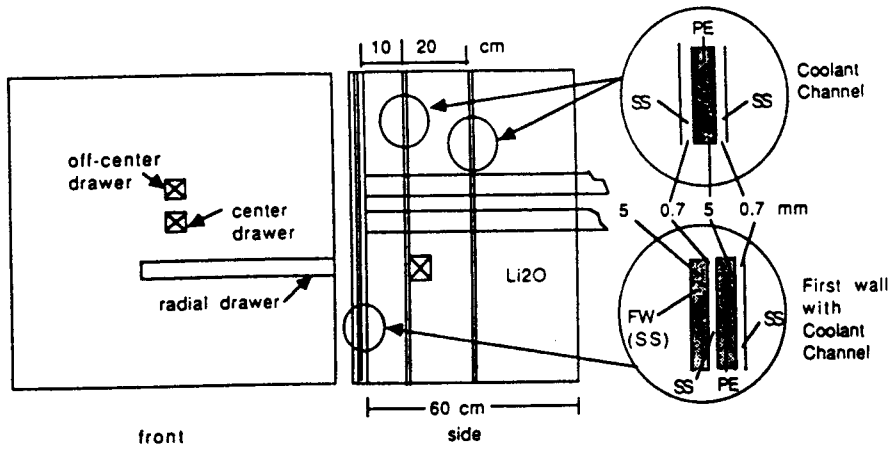

Fig. 10. The WCC experiment (Phase-IIC).

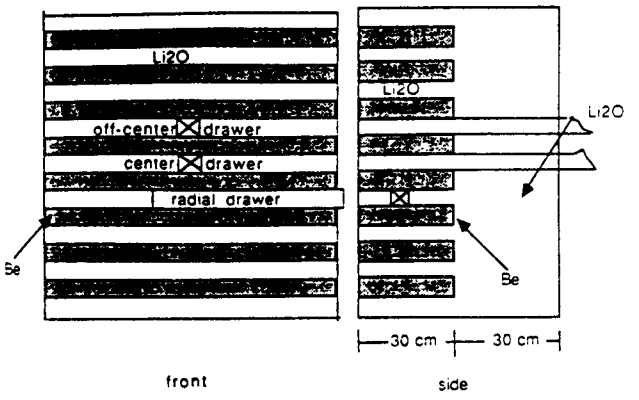

Fig. 11. Beryllium edge-on experiment (Phase-IIC).

Phase-IIC experiments, three horizontal drawers were utilized for axial measurements, as shown in Figs. 10 and 11.

III.B.3. Phase-III Experiments

In Phase-II, the neutron energy spectra in the plasma chamber were successfully simulated using a point neutron source inside a closed geometry assembly. However, the angular and energy distributions of neutrons incident on the first wall in magnetic fusion systems are produced by a volumetric source in the plasma region and could not be simultaneously simulated well with a point source. Furthermore, the uniformity of the spatial distribution of the nuclear responses in the toroidal direction of a tokamak could not be reproduced with a point neutron source. The point source could simulate an inertial fusion system but not a magnetic confinement system. The neutron angular distribution at the first wall has a substantial impact on reaction rates in the first wall and the regions immediately behind it. The need to better simulate simultaneously the neutron angular and energy distributions at the first wall and the uniform spatial distribution in the toroidal direction of a tokamak motivated the conception of the line source experiments in Phase-III. Because cost considerations precluded an actual line source, the point neutron source was cleverly utilized to realize a pseudo-line source. A continuous back and forth straight-line motion of the blanket test assembly relative to the fixed point source provided a line source neutronics effect using time averaging of the response of detectors, which were fixed inside the assembly and hence were moving together with the assembly.[34-37] The linearity of the neutron transport equation allows the superposition of the effects of the many point sources that simulate the line source and, hence, this time-averaging for nuclear responses that depend only on primary neutron reaction rates, e.g., tritium breeding and direct nuclear heating. However, for time-dependent responses such as induced activation, a more detailed treatment was necessary, particularly for isotopes with short decay lives.

Two operational modes, stepwise and continuous, were applied for movement of the test assembly to create the pseudo-line source effect. In the stepwise mode, the carriage deck on which the test assembly was loaded was stopped every 50 or 100 mm over its 2-m path length during the pause, and the source position was recorded. In the continuous mode, the test blanket was moved back and forth continuously with a constant speed of 6.1 mm/s. The position of the carriage deck and the neutron yield were recorded every 10 s. The stepwise mode was used for on-line measurement techniques, e.g., NE-213, Li-glass scintillators, and proton recoil gas proportional counters (PRCs). The continuous mode was utilized for passive measurement techniques, e.g., activation foil measurements requiring high neutron fluence.

Three experiments (IIIA, IIIB, and IIIC) were conducted during Phase-III using annular blanket assemblies and the pseudo-line source. Figures 12, 13, and 14 show the configuration, materials, and dimensions in Phases III-A, III-B, and III-C, respectively.[37]

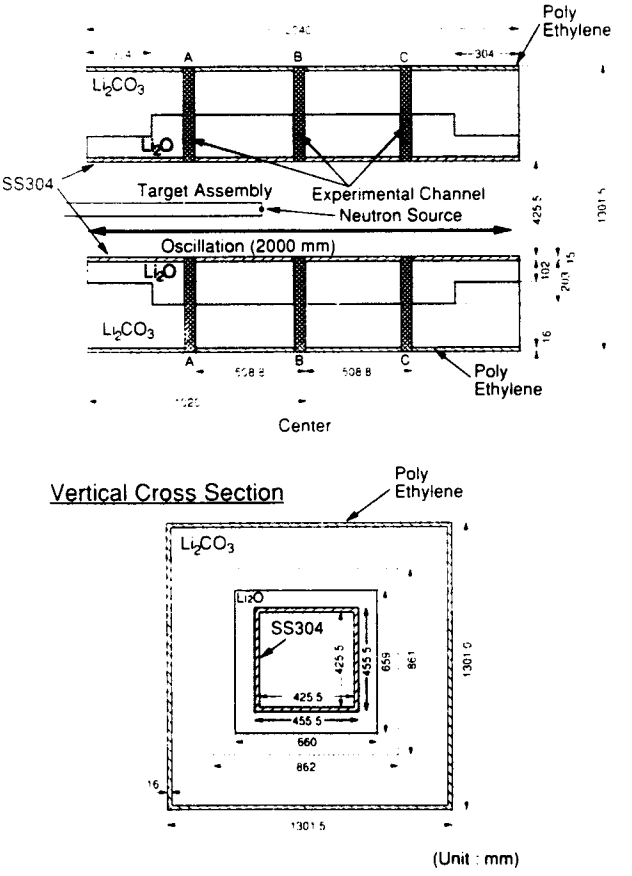

Fig. 12. Phase-IIIA experimental arrangement.

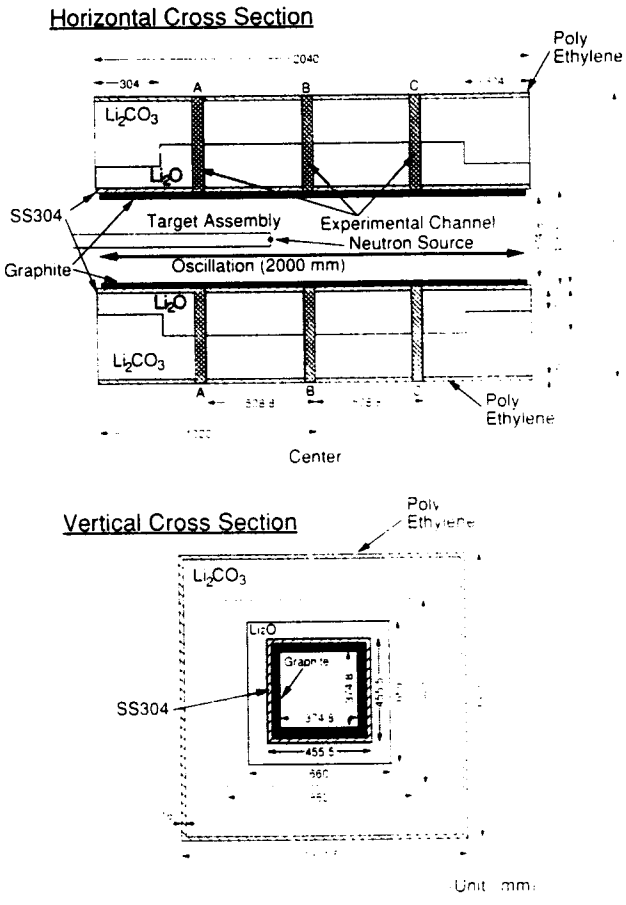

Fig. 13. Phase-IIIB experimental arrangement.

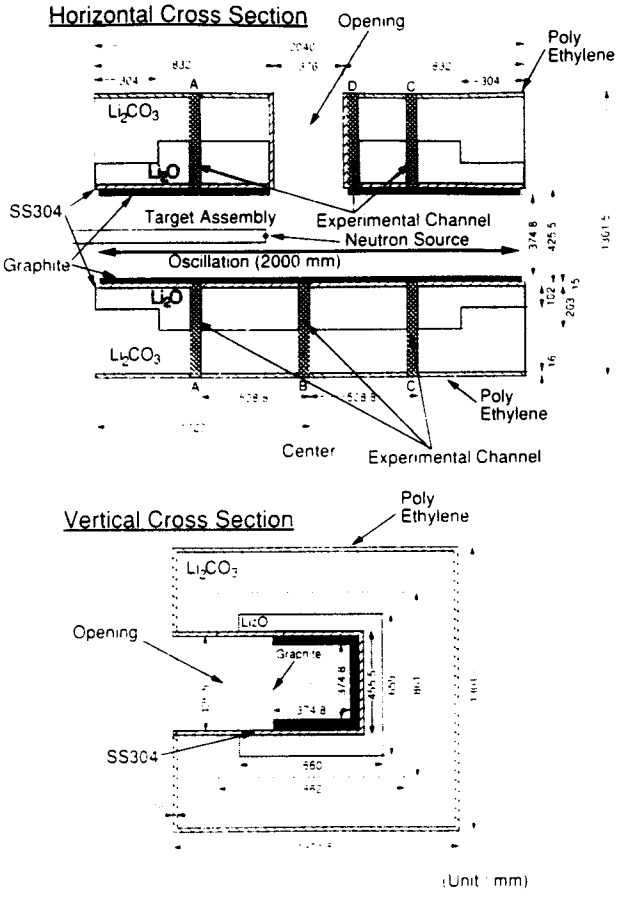

Fig. 14. Phase-IIIC experimental arrangement.

In Phase-IIIA, the test assembly (called reference test blanket) was made with a simple configuration simulating only the first wall and the Li_2O breeder zone. To reduce the effects of room-returned neutrons on the Li_2O test zone, Li_2CO_3 was placed outside the Li_2O. Three experimental channels were placed horizontally in each side of the assembly for in situ measurements.

In the Phase-IIIB experiment (see Fig. 13), a 25.44-mm-thick layer of carbon was placed in front of the first wall to simulate plasma-facing tiles or armors adopted in some fusion reactor designs.

In Phase-IIIC (see Fig. 14), a large opening 376 × 425 mm was made on one side of the test assembly of Phase-IIIB. The opening was lined with 15-mm-thick Type 304 stainless steel. This opening is representative of the many large openings for plasma heating, vacuum pumping, and other penetrations in fusion systems. One of the experimental channels was moved adjacent to the opening, as shown in Fig. 14.

III.B.4. Summary of Configurations and Materials

Figure 15 provides a schematic comparison of the experimental arrangement in Phases-I, -II, and -III. Table II highlights the primary features of the experiments in the three phases. We provide comprehensive details about all specific aspects of the experiments and measurement techniques in Refs. 25 through 39.

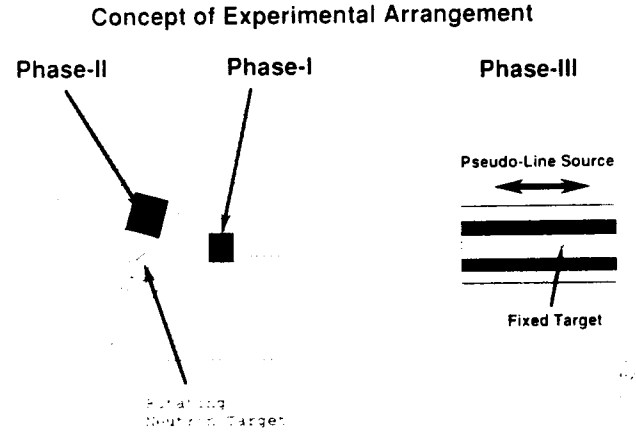

Fig. 15. A schematic comparing experimental arrangements for Phases-I, -II, and -III.

TABLE II

Summary of Key Features of Experiments in the Neutronics Integral Experiments Performed in Phases-I, -II, and -III

	Phase-I	Phase-II	Phase-III
Neutron source Shape of blanket test module	Point Cylinder	Point Rectangular	Line Annular
Overall configuration	Open geometry (neutrons can return from room wall to the face of test module)	Closed geometry (neutrons reach the test module either directly from the source or reflected from Li_2CO_3 enclosure)	Finite cylinder (neutrons reach the front of the test assembly either directly from the source or reflected from other parts of the test module)
Shortest distance from source to the face of test module (m)	2.5	0.78	~0.2
Breeding material in the test module	Li_2O	Li_2O	Li_2O
Neutron multiplier (only in some experiments)	Beryllium	Beryllium	
Relevant simulation to fusion reactors	Breeding test module in a shield blanket	Good simulation of neutron energy distribution in fusion system and good simulation of angular distribution in inertial fusion systems.	Good simulation of neutron energy spectra and improved simulation of angular neutron distribution in magnetic fusion systems.

III.C. Measurement Techniques

One of the most valuable results of the collaborative program is the development and application of several measurement techniques.[26] The nuclear parameters that received primary focus in the measurements included TPR, neutron spectra, foil activation reaction rates, nuclear heating, and induced radioactivity and decay heat. The measurements of the total nuclear heating were conducted in specialized experiments. The experimental measurements of induced radioactivity and total nuclear heating are summarized in separate sections. Below, a summary of the primary measurements for tritium breeding, neutron spectra, and reaction rates is given.

III.C.1. TPR

Because verification of data and codes for tritium breeding was a central focus in most of the integral neutronics experiments of the three phases, several measurement techniques were applied to obtain TPRs.

1. *Li-metal foil:* The liquid scintillation counting method with Li-metal foil is a passive method that relies on counting tritium beta decay after irradiation of samples. Enriched ^6Li, ^7Li, and natural Li-metal samples were encapsulated in pure aluminum. The overall error in the tritium production measurement is estimated to be ~5%.

2. *Li_2O pellet:* Except for the chemical processes, this technique is similar to that of the Li-metal foil. However, because Li_2O is the same material as that in the blanket test assembly, concerns about self-shielding within the pellet are reduced. The overall error with this technique is estimated to be ~5%.

3. *Li-glass detector:* The events by the $^6Li(n,\alpha)^3H$ reaction are directly counted by a pair of ^6Li- and ^7Li-glass detectors. The gamma-ray background is subtracted by the ^7Li-glass response. This technique can provide the reaction rate in real time. The overall absolute error is estimated to be 3 to 6%.

4. *Li_2O block (zonal method):* In this method, Li_2O blocks similar to those of the breeding material are used as detectors rather than the foregoing techniques in which small pellets used as detectors are placed between the stacked Li_2O breeding material blocks. This method provides a higher accuracy of a region-integrated TPR. It also sharply reduces the uncertainty associated with a small detector location in a region with steep gradients. The overall error with the Li_2O zonal method measurements is estimated to be ~3%.

5. *indirect methods:* The TPR from the threshold reaction $^7Li(n,n'\alpha)t$ was indirectly derived using the neutron spectrum measured by a small sphere NE-213 scintillation spectrometer. Because this method relies on the use of the cross-section data for $^7Li(n,n'\alpha)t$ from evaluated data, it does not provide direct experimental verification of the integrated tritium production from ^7Li.

III.C.2. Reaction Rates

The well-established passive dosimeter method of foil activation was used to measure reaction rates

for $^{27}Al(n,\alpha)^{24}Na$, $^{58}Ni(n,2n)^{57}Ni$, $^{58}Ni(n,p)^{58}Co$, $^{93}Nb(n,2n)^{92m}Nb$, $^{115}In(n,n')^{115m}In$, and $^{197}Au(n,\gamma)$-^{198}Au. Because the thresholds of these reactions are different, they are used as spectral indices to validate neutron spectrum measurements. The small size of the detector foils allows good spatial resolution and small perturbation of the field. The overall experimental error ranged from 3 to 6%.

III.C.3. In-System Neutron Spectra

A 14-mm-diam spherical NE-213 liquid scintillator was used to measure the fast neutron spectrum above 2 MeV at several locations inside the system. The overall experimental error was estimated to be ~4% for the flux above 10 MeV and ~10 to 20% for that from 2 to 10 MeV.

Neutron spectra from a few kilo-electron-volts to 1 MeV were measured using a newly developed small-sized PRC. The overall error in PRC measurements was estimated to be ~3 to 10% above 10 keV.

III.C.4. Nuclear Heating Experiments

Attempts started in 1988 to perform integral experiments to verify data and codes for nuclear heating predictions.[29,30] Performing such measurements inside the experimental assemblies of Phases-I, -II, and -III, described earlier, was not feasible except by gamma-ray heating measurements because the nuclear heating rate especially by neutron interaction was too difficult to measure using the state-of-the-art techniques.

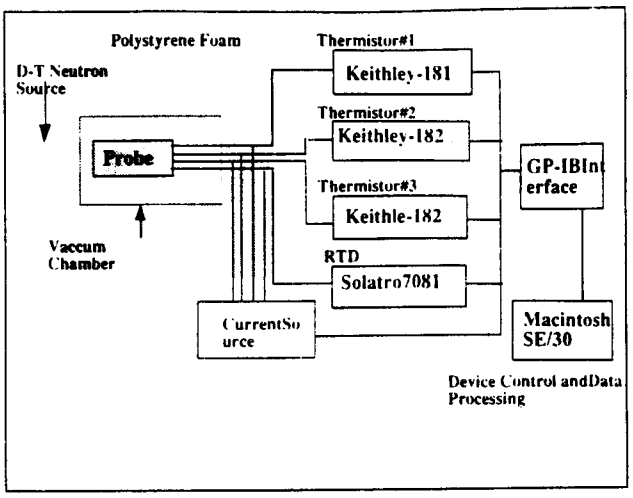

Fig. 16. Block diagram of nuclear heating measurements.

To provide direct measurements of total nuclear heating, special experiments were performed using an improved microcalorimeter.[29,30] A block diagram of the nuclear heating measurement system is shown in Fig. 16. A single probe configuration was used for a single material. A series of experiments was conducted with different materials. The probe materials were put in a vacuum chamber suspended with thick carbon papers. A schematic cross-sectional view of the microcalorimeter is given in Fig. 17. The microcalorimeter

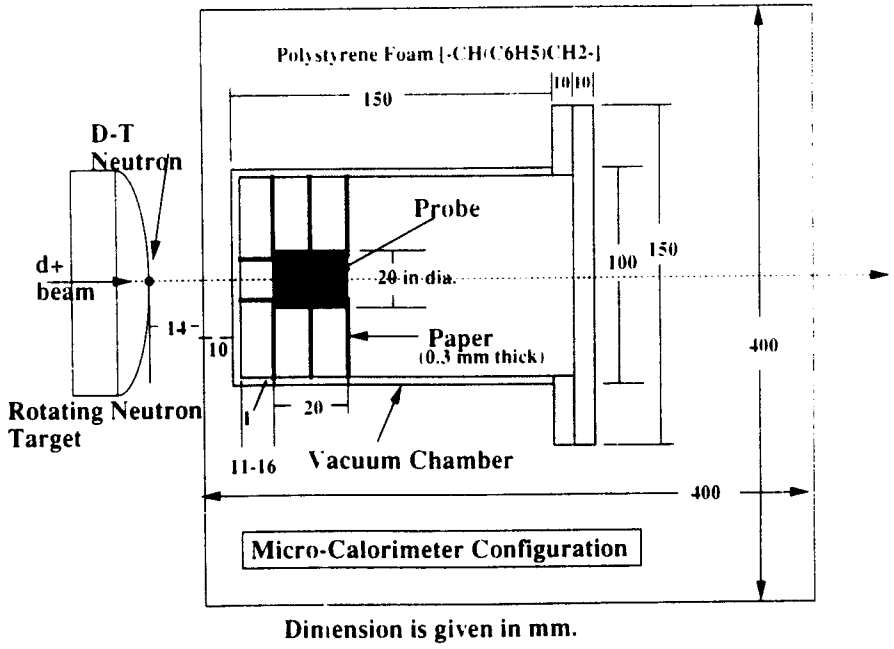

Fig. 17. Microcalorimeter configuration.

technique consists primarily of two components: the material in which radiation energy is produced and absorbed, thus generating heat, and a thermal sensor for detecting temperature rise due to the heat generation. Bead (point-size) thermistors and platinum resistance temperature detectors were employed as thermal sensors.

Note that the nuclear heat generation rate obtained in the experiments was small, typically $\sim 10^{-4}$ to 10^{-5} W/g, which was smaller than the typical 10^{-3} W/g joule heating in the electric resistance of the thermistor sensor. The temperature change due to nuclear heating was very small, $\sim 10^{-4}$ to 10^{-5} K/s. The probe was located at a distance from the neutron source of ~35 to 45 mm. A significant fraction of the nuclear heating in the probe material came from gamma rays produced in the neutron source target assembly.

It is encouraging that nuclear heating measurements were conducted with reasonable success. Prior to these measurements, there was no experimental data for direct nuclear heating in a simulated fusion environment. The difficulties that had to be overcome were great, given the limited yield of the neutron source and, hence, the very small nuclear heating and the correspondingly small temperature rise.

Analysis of experimental errors identified the following sources of uncertainties: (a) neutron flux determination (probe position, absolute neutron yield, cross-section data, and transport calculations), (b) net temperature rise derivation, (c) conversion coefficient of sensors, and (d) heat gain and losses through conduction, convection, and radiation. Using standard statistical methods, the overall experimental error was estimated[29,30] to be ±10%.

In addition to the single-probe experiments, an additional nuclear heating experiment was conducted using an assembly made of a Type 304 stainless steel core enclosed in Li_2CO_3 blocks. The nominal size of the Type 304 stainless steel core was 357 × 458 × 458 mm. The front surface of the assembly was placed close to the D-T neutron source to maximize the neutron flux level. Thermal sensors were placed inside the Type 304 stainless steel core.

III.D. Induced Radioactivity and Decay Heat Experiments

The integral experiment setup of the collaborative program provided a powerful and unique opportunity to directly measure the total level of induced radioactivity in fusion spectra. As discussed earlier, the neutron spectra in the experimental assemblies of Phases-II and -III are essentially similar to those in the plasma chamber and first-wall/blanket region of fusion systems.

A number of experiments were conducted in Phases-IIC and -III to determine the integral radioactivity characteristics of a number of materials in the fusion-like spectra near the first wall and inside the blanket.[27,28] For example, in the Phase-IIC experimental arrangement shown earlier in Fig. 10, specimens were located at two locations: A and B. Location A is located inside the simulated plasma chamber region 100 mm from the source. Location B is inside the Li_2O test module ~820 mm from the source and 50 mm deep into the Li_2O region. Two irradiation schemes of short for 30 min and long for 10 h were applied for both A and B sample positions.

Emission rates of gamma rays from decaying radionuclides were measured at different times during cooling-off periods after the neutron irradiation. The gamma-emitting radioactive isotopes generally span a huge range of half-lives, extending from a fraction of 1 s to 1 million yr. However, practical considerations related to the availability and capability of the neutron source and gamma detectors as well as to available manpower limited the focus of this program to radioisotopes with half-lives in the range of a few minutes to a few years. The cooling times after irradiation for decay gamma measurements ranged from 10 min to several hours for short irradiation and from 1 h to several days for long irradiation. Many materials of interest to fusion applications were investigated.

III.E. Calculational Methods

Comprehensive calculations and analyses were performed prior to and after carrying out the experiments. The pre-experiment analysis focused on planning and design of experiments including choice of geometry, configurations, materials, and location of detectors. The postexperiment analysis aimed at comparing and interpreting the experimental and calculation predictions and identifying sources of discrepancies and deficiencies in nuclear data libraries and neutronics codes.

State-of-the-art codes and libraries were used. Some of these codes and data libraries evolved over the 10-yr period, in part to correct deficiencies uncovered in the collaborative program. Therefore, the versions of the codes and libraries used in the analysis changed with time. Detailed accounts of the exact versions of the codes and libraries used are given in Refs. 25 through 39. Here, we make a brief statement of the codes and libraries used.

Much of the analyses were carried out by two groups, one at JAERI and the other at UCLA. Both deterministic and Monte Carlo methods were used to predict the neutron, and in some cases the photon, transport. The United States adopted the MCNP-3B Monte Carlo code, which uses continuous energy and angle treatment and ENDF/B-V data. In contrast, JAERI utilized either the MORSE-DD Monte Carlo code, which uses multigroup treatment, or its vectorized version, called GMVP. Both codes were used with the DDXLIB-J3 library, which was derived from JENDL-3.

For deterministic transport calculations, the United States utilized the DOT 5.1 discrete ordinates code along with the RUFF first-collision code. The cross-section library used with DOT was the MATXS6 library, which was based on ENDF/B-V. In the JAERI

analysis, DOT 3.5 was used along with the FNSUNCL code. The latter is a modified version of GRTUNCL and treats multiple neutron sources, including variations in energy and angle distributions. The FUSION-J3 library based on JENDL-3 data was used with the DOT 3.5 calculations.

The tritium production per source neutron per unit volume was calculated according to Eqs. (5), (6), and (7). Reaction rates for other neutron-induced reactions were calculated in a similar fashion. Detailed calculational issues such as correction for size of detectors, self-shielding approximations in geometrical representation, order of $S_n - P_n$ approximations, and Monte Carlo statistics are treated in Refs. 5 through 39.

IV. HIGHLIGHTS OF MAIN RESULTS AND LESSONS LEARNED

Experimental measurements were obtained using various measurement techniques during Phases-I, -II, and -III. The results were analyzed in detail by the UCLA and JAERI groups. The detailed results of the measurement and analyses are reported in Refs. 25 through 39. Here, we summarize some of the key results and provide an overall interpretation of their significance to predicting tritium breeding, total nuclear heating, and induced radioactivity in fusion systems. We also provide some additional remarks that are important to future fusion neutronics efforts based on lessons learned from the overall results of the collaborative program.

IV.A. Neutron Source

Compared with other accelerator-based point neutron sources in the world, the FNS facility has some of the strongest capabilities. The water-cooled rotating target can provide a yield up to $\sim 5 \times 10^{12}$ n/s. The stationary target at FNS has a yield up to $\sim 3 \times 10^{11}$ n/s.

The FNS neutron source has proved adequate for moderately complex integral experiments for measurements of tritium production, measurements of induced radioactivity for radioisotopes with short-to-medium (several years) half-lives, and shielding experiments in which radiation is attenuated by no more than about five orders of magnitude.

While FNS has the best capabilities in the world now, it still has limitations, and it cannot adequately address all the fusion neutronics issues. In particular, a much higher neutron yield is needed to perform integral neutronics experiments with the complexity that exists in fusion reactors. For example, some key shielding issues involve 10 to 15 orders of magnitude attenuation (e.g., the biological dose outside the reactor building). While the success in nuclear heating measurements at FNS during the collaborative program is encouraging, the limited neutron yield produces only $\sim 10^{-5}$ K temperature rise in a small probe. Better experimental data on nuclear heating in prototypical assemblies require much higher neutron yield.

One of the lessons learned in the collaborative experiments is the trade-offs between the neutron yield and complexity. Increasing the neutron yield requires a cooled rotating target. This reduces the flexibility and increases the effort to achieve accurate source characterization. In addition, a higher neutron yield requires that the walls of the room that houses the target and experimental assembly be made thicker, and the room is often made smaller in order not to increase cost. For example, the significant achievement of simulating the line neutron source in Phase-III was accomplished using the lower neutron yield stationary target rather than the higher yield rotating target, which was too complex to use in the required, precise axial movement, particularly in the small space available in the target room.

IV.B. Neutron Spectra and Angular Distributions

Neutrons produced in D-T fusion reactors are essentially isotropic and have a narrow energy distribution at ~14 MeV. The energy and angular distributions of the source neutrons incident on the first wall depend on the fusion reaction chamber volume, geometry of the system, and other parameters. There are major differences between the IFE and the MFE systems. For the IFE systems, the neutron source is essentially a point at the center of a sphere (or at the center of a cylinder). In a tokamak, there are a number of important features of the neutron source: It has (a) a spatial distribution inside the volume of the plasma, (b) the presence of the scrape-off region between the edge of the plasma and the first wall, which is essentially void, (c) toroidal curvature, and (d) uniformity in the toroidal direction (i.e., toroidal axis symmetry). An example of the consequences of such neutron source characteristics is a special angular distribution; for example, the angular flux of the virgin neutrons incident on the first wall increases with increasing angle (where the angle of incidence is measured in the midplane from the direction perpendicular to the first wall), and then it starts to decrease beyond a certain angle until it becomes zero at an angle significantly smaller than 90 deg. Such an angular distribution of the source neutrons incident on the first wall affects the reaction rates in the first wall and in the front regions of the blanket.[61,62]

The energy distribution of fusion D-T neutrons can be conveniently reproduced with a D-T point neutron source. However, the angular distribution incident on the first wall is difficult to reproduce with a point neutron source for at least two reasons: (a) the use of a single beam directed at the target and (b) the geometry of the assembly relative to a point source. Table III shows the calculated energy and angular distributions of the emitted D-T neutrons from the rotating target (Phase-II

TABLE III

Energy and Angular Distribution of the Emitted (D-T) Neutron

E (MeV) Upper	$S(\mu)$[a]	Angle $\mu = \cos\theta$[b]						
		−0.940	−0.707	−0.259	0.259	0.707	0.940	1.0
15.49	0.302						0.293	0.707
15.25	1.666					0.010	0.700	0.290
15.01	4.174					0.241	0.587	0.172
14.78	7.641					0.517	0.406	0.077
14.55	9.293				0.085	0.798	0.111	0.006
14.32	9.469				0.746	0.250	0.003	0.001
14.10	9.225			0.070	0.930			
13.88	8.882	0.001	0.033	0.939	0.027			
13.67	7.880	0.049	0.376	0.575				
13.46	4.313	0.184	0.698	0.118				
13.25	1.193	0.559	0.441					
13.04	0.031	1.000						
12.84								
Total[c]		0.028	0.108	0.215	0.260	0.233	0.123	0.032

[a]Energy distribution of source integrated for cosine of angle, $\mu = \cos\theta$.
[b]θ is the angle with the D^+ beam.
[c]Normalized to unity.

experiments). The neutrons are emitted with a high degree of anisotropy as compared to nearly isotropic production in the plasma. The second effect, i.e., the effect of the geometry and configuration of the assembly relative to the source geometry, compounds the difficulty of reproducing the angular distribution of the source neutrons at the first wall. Considerable improvements in this area were achieved by the line source simulation in Phase-III compared with the point source simulation in Phase-II.

Because the angular distribution cannot be reproduced correctly with accelerator-based neutron sources, the absolute magnitude and the spatial distributions of the neutron reaction rates in the first wall and the front blanket regions cannot be compared directly to that in a fusion reactor. The benefit of the integral experiments in this case is to verify basic data and calculational methods rather than provide direct measurements for use in reactor designs. However, even in this case, it is important that some figures of merit are used to indicate the degree of similarity between the experiments and fusion systems. One such figure of merit is the volume-integrated spectrum, which includes not only the source neutrons but also all scattered neutrons. Figure 18 compares the volume-integrated spectra calculated for representative first-wall/blanket systems in typical magnetic fusion reactors to those obtained in the reference assemblies of Phases-IIB and -IIIA. The comparison shows that the general features of the spectra can be reasonably reproduced in the integral experiments.

IV.C. Closed Versus Open Geometry

As mentioned earlier, the Phase-I arrangement is called open geometry. The face of the experimental

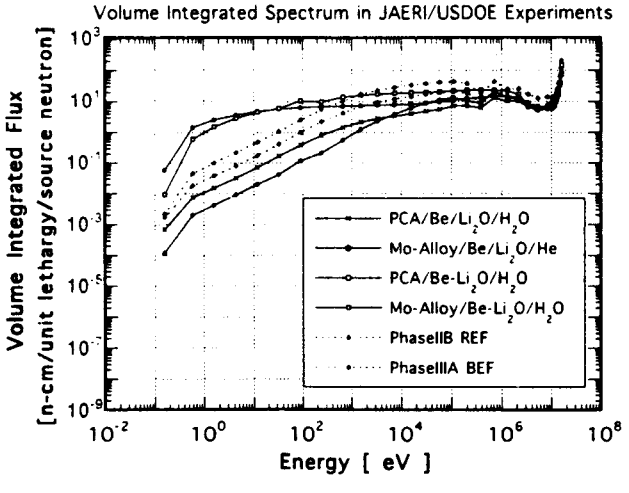

Fig. 18. Comparison of the volume-integrated neutron source spectra of representative reactors with some of the experimental systems of the collaborative program.

blanket module is open to room-returned neutrons in addition to direct source neutrons. Figure 19 shows an example of the ratio of the calculated-to-measured (C/E) values of the local TPR in Phase-I. The C/E value grossly deviates from unity at the front locations. The deviation is much larger in the front region than in the deeper regions of the test assembly because of the difficulty of predicting the room-returned neutron component.

Much better results were obtained in Phases-II and -III, as will be discussed shortly, when a closed geometry was used. In a closed geometry, the source is surrounded by a breeding material, and only a very small number of room-returned neutrons reach the front regions of the blanket test assembly.

While the lesson here is that integral neutronics experiments should be performed in closed geometry, the results of Phase-I remain a concern. Tokamaks have very complex geometries with many components and a diversity of construction materials. The inability to correctly predict the radiation field of the room-returned neutrons from the much simpler geometry of the target room 2 at FNS is a serious reminder of the limitations of current transport codes and nuclear data. Given such experience, it is not clear that the biological dose outside the reactor building of a tokamak reactor, for example, can be reliably predicted using present codes and data.

IV.D. Accuracy of Measurement Techniques

One of the most important contributions of the collaborative program is the development of measurement techniques. Table IV compares the experimental error obtainable with various tritium production techniques. Tritium contamination of the samples of passive methods is sometimes found in scintillation counting. Zonal measurements provide the smallest uncertainty of all

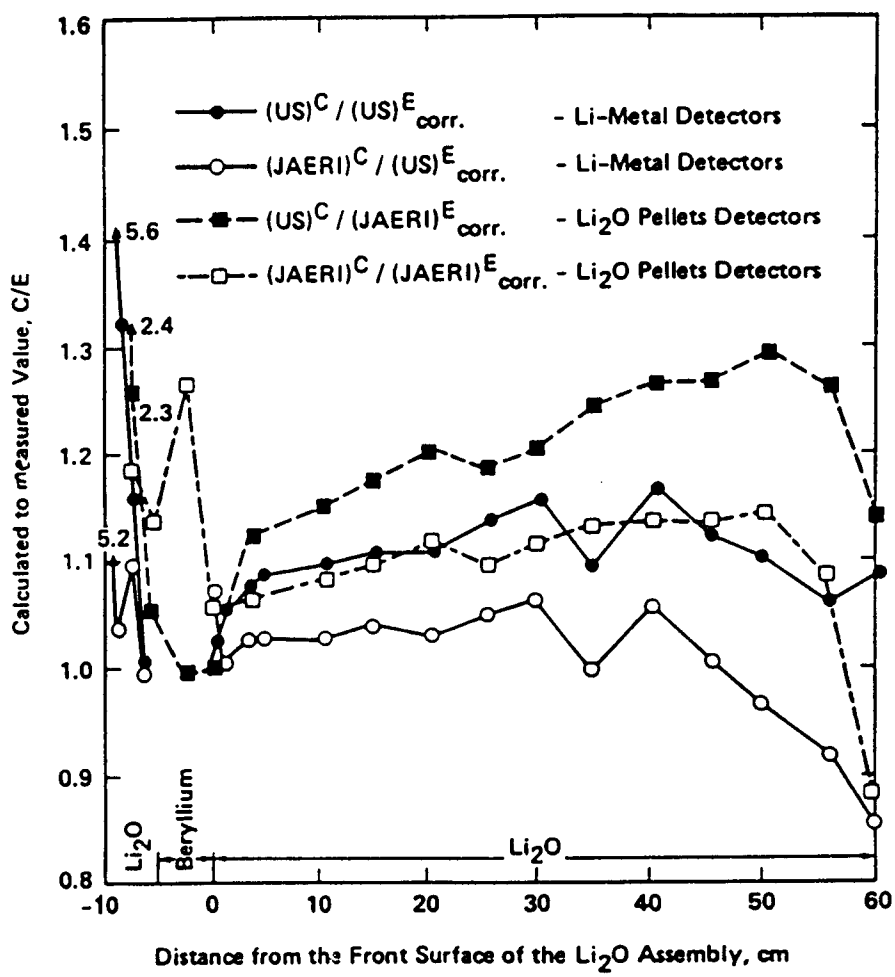

Fig. 19. The C/E ratio for TPR from ^{6}Li (T_6) in the beryllium-sandwiched system of Phase-I based on DOT calculations and Li-metal and Li_2O pellet measurements.

TABLE IV

Comparison of Experimental Errors Among Tritium Production Measurement Techniques

Method	Approximate Measurement Error (%)	Comments
Passive (postprocessing) methods		
Li-foil	5	Protection from tritium contamination is necessary; high fluence is required.
Li_2O-pellet	5	Protection from tritium contamination is necessary; high fluence is required.
Li_2O-zonal	3	Modest fluence.
LiF-TLD	10 to 20	Relative measurement only.
Active (on-line) methods		
NE-213	5 to 8	Depends on cross-section data used; void effect should be considered.
Li-glass	3 to 6	Void effect should be considered.

techniques because of a good signal-to-background ratio, but the spatial resolution is poor. Figure 20 shows the comparison of the results among three different techniques obtained in the Li_2O test blanket in Phase-IIA. There is ~5 to 10% discrepancy among the three techniques, which is slightly larger than the experimental error.

In summary, the best present measurement techniques are limited in accuracy with ~3 to 5% error for tritium production, 5 to 10% for neutron spectrum, 3 to 6% for activation reactions, and 10 to 20% for gamma-ray heating rates. The limitation on the accuracy of measurement techniques is one of the factors that must be accounted for in the design. For example, a minimum of 5% margin in the TBR is necessary for all breeding blanket designs to account for inaccuracies in measurement techniques alone.

A critical point must be made concerning future measurements in fusion devices. Most of the present measurement techniques cannot be applied in fusion devices where high temperatures and high magnetic fields exist. Therefore, the development of new measurement techniques is needed for neutronics experiments in fusion devices such as ITER.

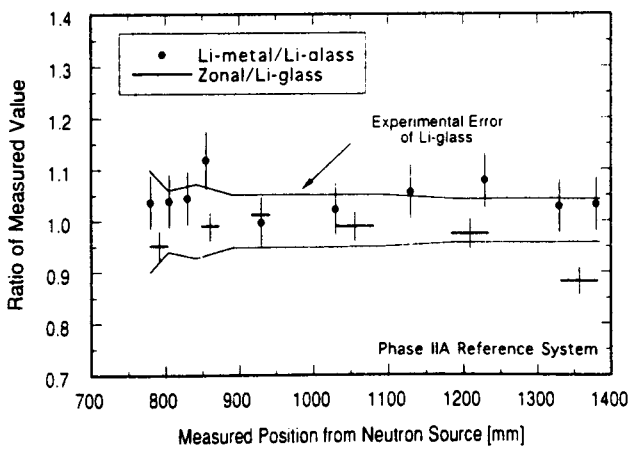

Fig. 20. Comparison of measured values for ^6Li TPRs obtained with different techniques.

IV.E. Tritium Production Prediction

Comparison of the results of experimental measurements to those obtained using calculational codes and basic nuclear data provides an important indication of the accuracy of calculations. As indicated earlier, the many experiments conducted in Phases-I, -II, and -III were analyzed in detail and are presented in a number of papers (see, for example, Refs. 5 through 39). Here, we present limited examples to show the present uncertainty in calculating tritium breeding.

Figure 21, based on DOT 5.1 calculations, shows TPRs from ^6Li (T_6) and from ^7Li (T_7) along the central axis of the WCC experiment conducted in Phase-IIC, described earlier in Sec. III. The results show that the T_7 profile is somewhat smooth, but the T_6 profile is very steep at the boundaries of the interface between the Li_2O and the WCC. The reason is that the neutron spectrum inside and around the coolant channels has a large component of low-energy neutrons produced by neutron moderation in the hydrogen-containing coolant. The ^6Li tritium-producing reaction cross section increases at lower neutron energies.

Figure 22 shows the C/E values of TPR from ^6Li (T_6) measured by Li-glass detectors along the central axis in the WCC experiment. Four curves are shown in

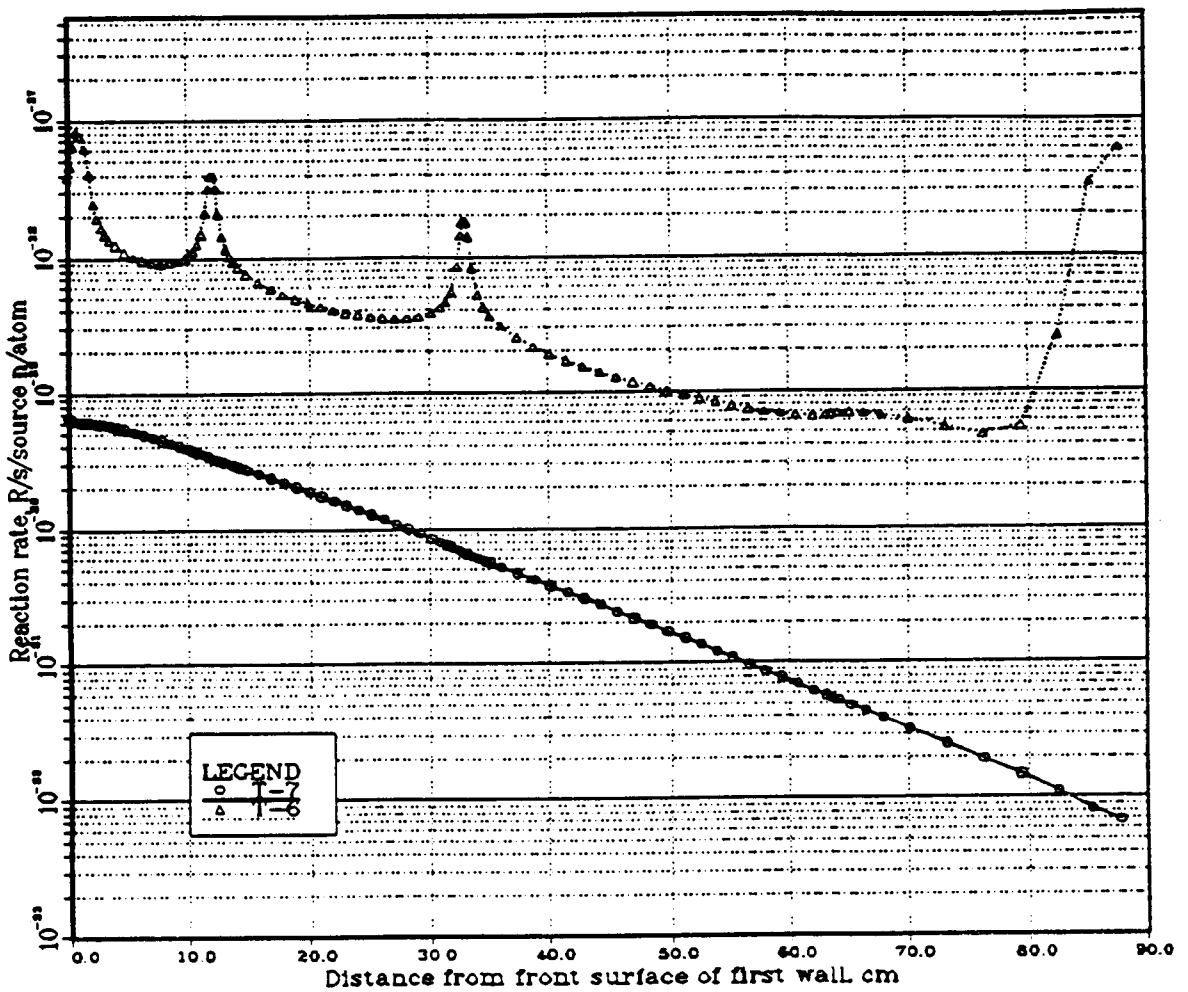

Fig. 21. The TPRs from ^{6}Li (T_6) and ^{7}Li (T_7) along the central axis of the WCC experiment in Phase-IIC.

Fig. 22, which correspond to the calculated values obtained using two discrete ordinate codes (DOT 5.1 and DOT 3.5) and two Monte Carlo codes (MCNP-3B and MORSE-DD) with different databases.[32] Important observations can be made on the results. First, the C/E values deviate from unity by ~5 to 10% in regions inside the Li_2O away from the coolant channels. Second, large discrepancies of ~20% between the C/E values are observed at the interfaces between the Li_2O and the coolant channels. Third, systematic differences appear between the Monte Carlo and the S_n calculations, and the statistical errors in Monte Carlo are relatively large.

Figure 23 shows the C/E values of TPRs from ^{7}Li (T_7) in the radial direction along drawer B of the Phase-IIIA measurements (described earlier in Sec. III), based on the NE-213 measurements. The C/E values in Fig. 23 are shown for several calculational results using Monte Carlo and discrete ordinates codes performed independently in the United States and JAERI. The C/E values lie between 0.9 and 1.05 indicating a prediction uncertainty in local T_7 of approximately −10 to +5%. Note that the MCNP calculations at $R = 545.8$ mm have a large statistical error of ~12% and were not considered in these estimates. The corresponding results for T_6 in the same drawer are shown in Fig. 24, where the measurements are based on Li-glass. The C/E values are generally larger than unity by 5 to 15%.

It is common in literature to use the C/E ratio as a parameter to measure the quality of agreement between calculation and experiment. This parameter is very useful, but it is not totally satisfactory. For example, when the value of C/E is unity, it would seem to mean agreement, but it will also be 1 if the calculation and the experiment differ from their correct values by the same factor. Furthermore, C/E > 1 can occur because either the calculated value is too large or the experimental value is too small. Therefore, an evaluation methodology that considers errors in both experiments and calculation needs to be developed.

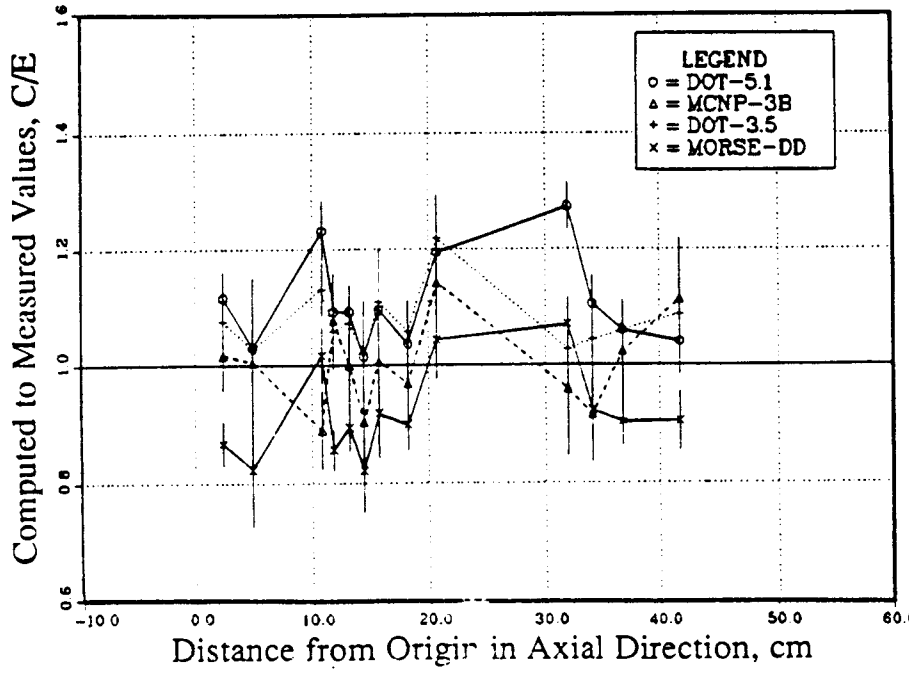

Fig. 22. The ratio of C/E values of TPR from ^{7}Li (T_7) measured by Li-glass detectors along the central axis in the WCC experiment.

An attempt was made to better quantify the prediction uncertainty in local and line-integrated TPR from ^{6}Li and ^{7}Li in all the integral neutronics experiments performed under the collaborative program. The details of the methodology are provided in Refs. 38 and 39. Briefly, the highlights of the method are as follows. The best-fitting curve (by the least-squares method) for the measured data is integrated in the axial (or radial) direction, and the uncertainty (error) in the line-integrated value E_{int} is estimated from the uncertainties in the fitting coefficients, which account for the uncertainty in the measured data. The same procedure is applied to the calculated values in obtaining C_{int} at the locations where the measurements are taken. An

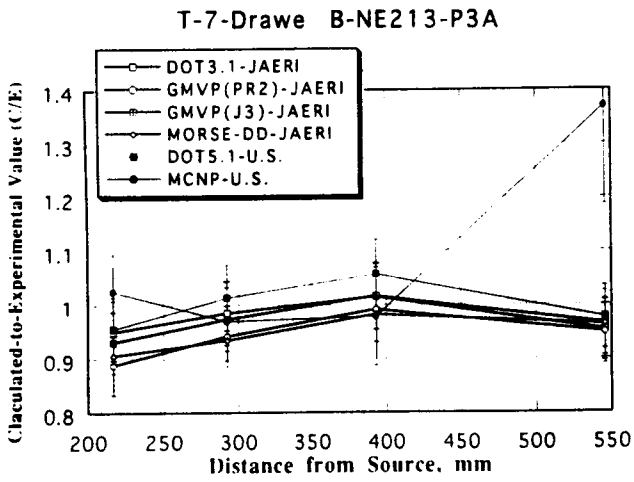

Fig. 23. The C/E values of TPRs from ^{7}Li (T_7) in the radial direction along drawer B of the Phase-IIIA measurements, based on NE-213 measurements.

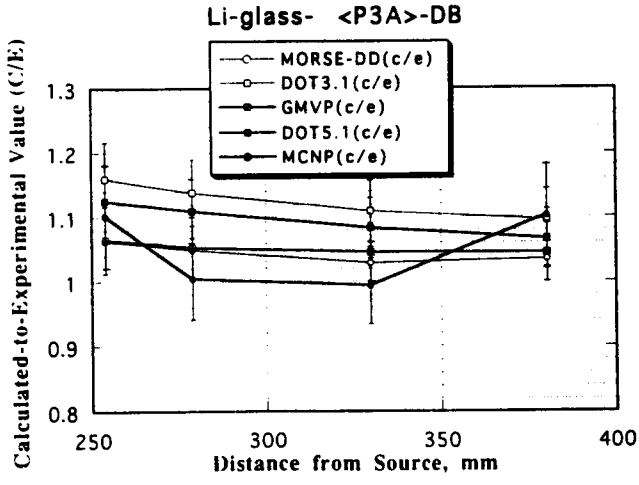

Fig. 24. The C/E values of TPRs from ^{6}Li (T_6) in the radial direction along drawer B of Phase-IIIA, based on Li-glass measurements.

estimate is then made for the value $(C/E)_{int} - 1$ and the associated relative standard deviation σ. These prediction uncertainties and associated errors serve as a good indicator to characterize the differences between calculations and measurements.

We present more detailed results on the prediction uncertainty for T_6 and T_7 for all measurement techniques and calculation methods in Refs. 38 and 39. Figure 25 shows the prediction uncertainty in the line-integrated TPR from ^{6}Li (T_6) based on measurements using the Li-pellet method. The results are shown for the Monte Carlo and discrete ordinates calculations in JAERI and the United States. The prediction uncertainty is given separately for various experiments conducted during Phases-I, -II, and -III, using the notation given in Sec. III to designate specific experiments. Figure 26 shows the prediction uncertainty in the line-integrated TPR from ^{7}Li (T_7) based on measurements using the Li-pellet method.

What is most striking about the results in Figs. 25 and 26 is that the prediction uncertainty varies not only among codes and data libraries but also from one experimental arrangement (configuration and materials) to another. Combining the results from all experiments and experimental methods to arrive at a composite prediction uncertainty is discussed in Ref. 39, where the composite prediction uncertainty in the line-integrated T_6 is calculated (based on U.S. codes and data) to be -5% with a standard deviation of $\pm 8\%$. The composite prediction uncertainty for the line-integrated T_7 is also -5% with a standard deviation of 11%.

Designers are generally interested in safety factors as a means to cover for uncertainty in calculations and design data. Such safety factors should depend, of course, on the specific calculation method and the details of the design. However, an attempt was made to derive safety factors based on all calculation methods and all experiments in all phases of the JAERI/U.S. collaborative program.[39] The results are summarized in Fig. 27, which shows the confidence level for calculations not to exceed measurements as a function of design safety factors. Separate curves are given for the United States, JAERI, and the combined U.S.-JAERI calculations for T_6, T_7, and tritium production from natural lithium (T_n).

In engineering applications, a 90% confidence level is generally applied. In this case, the safety factor shown in Fig. 27 ranges from -1.1 to 1.2. However, the safety factor needed increases significantly when a higher confidence level is applied.

There are critical issues here concerning whether the safety factor in Fig. 27 is sufficient and whether it is affordable. This safety factor is derived based on the integral experiments in Phases-I, -II, and -III. While these

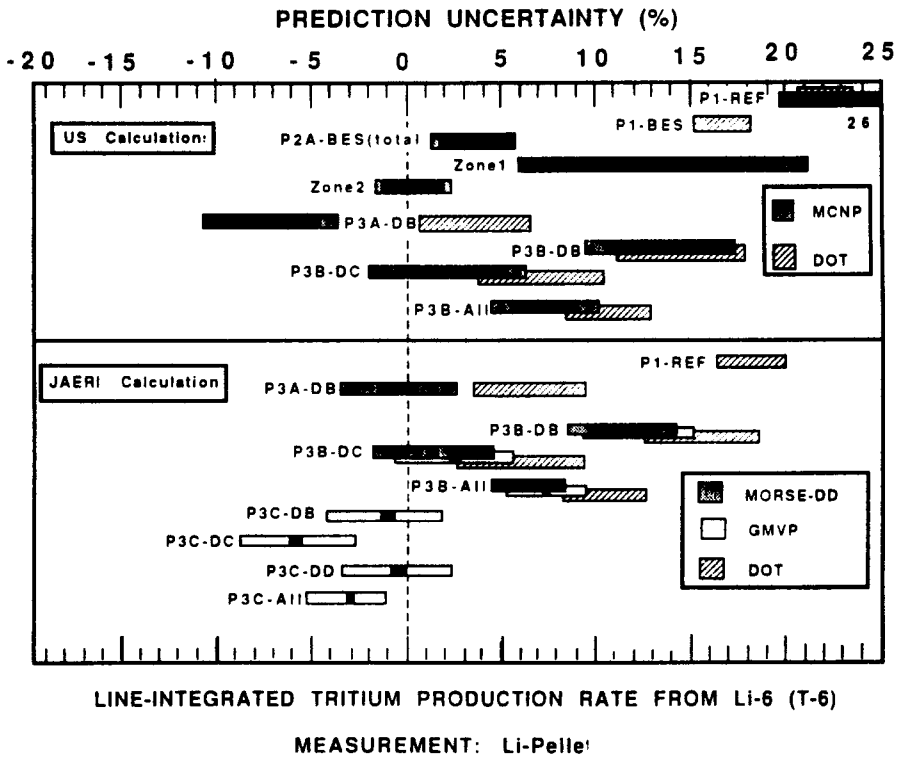

Fig. 25. The prediction uncertainty in the line-integrated TPR from ^{6}Li (T_6) (based on measurements using the Li-pellet method).

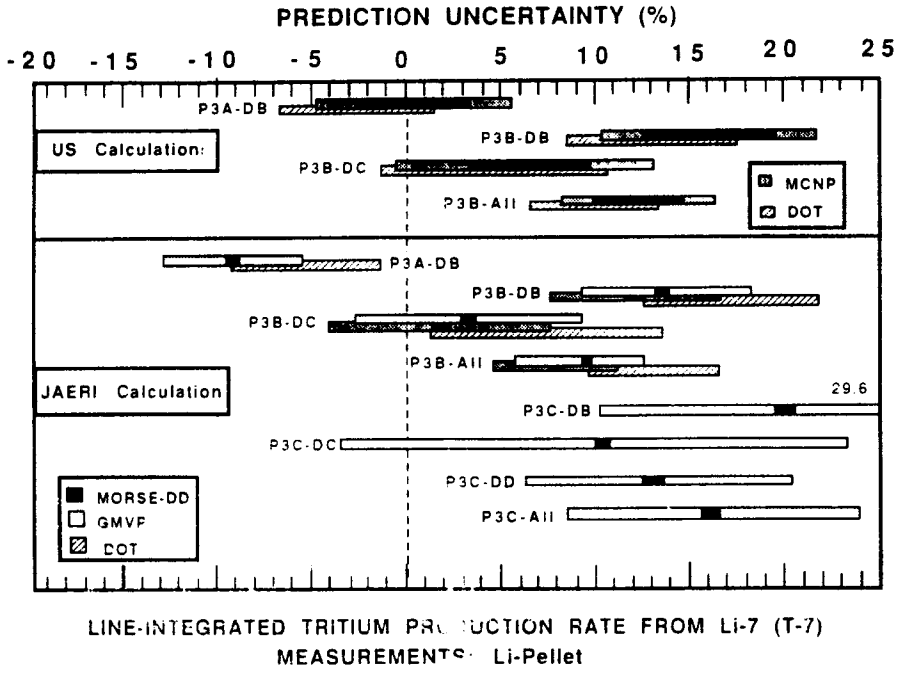

Fig. 26. The prediction uncertainty in the line-integrated T. from ^{7}Li (*T*-) (based on measurements using the Li-pellet method).

experiments represent a significant accomplishment, they still fall far short from representing the complex blanket geometry with a high degree of heterogeneity and a variety of void penetrations. Therefore, the safety factors in Fig. 27 should be used with caution as they may not be sufficient to cover all sources of uncertainties in a real fusion reactor system.

These safety factors do not appear to be affordable for most candidate blanket concepts in a tokamak system. For example, the most detailed recent European

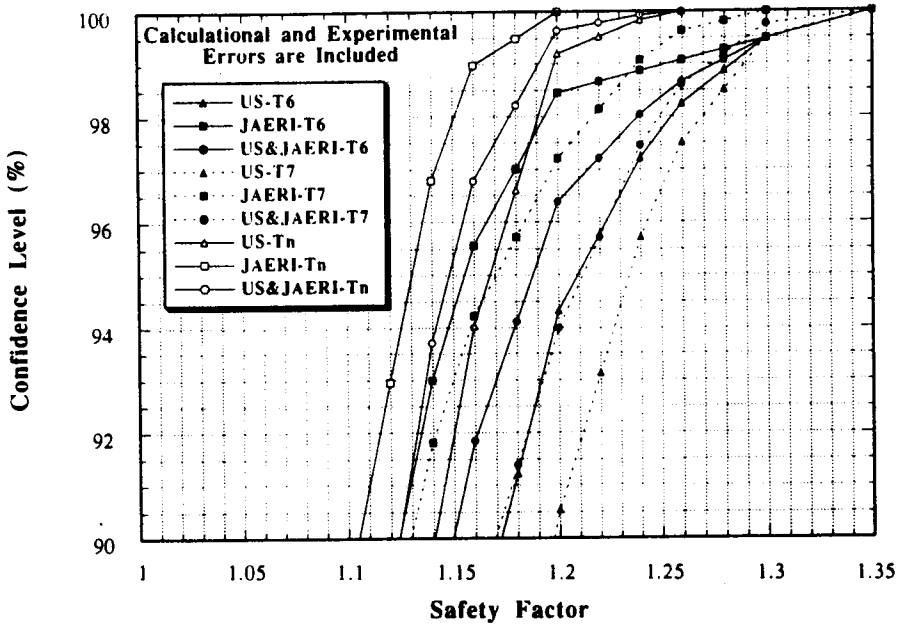

Fig. 27. Confidence level for calculations not to exceed measurements as a function of design safety factor, based on all calculation methods and all experiments conducted in all phases of the collaborative program.

blanket designs[63-66] have a maximum TBR of ~1.06 to 1.2. The TBR required for tritium self-sufficiency[67] is in the range of 1.05 to 1.3 depending on the tritium inventories in various components as well as on the desired doubling time. Therefore, it is not clear that a design window exists if a large safety factor is required.

An important overall conclusion, therefore, is that attaining tritium self-sufficiency cannot be guaranteed in present tokamak reactor conceptual designs using present candidate blanket concepts. Attaining tritium self-sufficiency is an absolute requirement in fusion systems operating on the D-T cycle. Therefore, R&D related to all aspects of tritium breeding, extraction, processing, and fueling must receive high priority. Actual demonstration of tritium fuel self-sufficiency should be a high priority in fusion testing facilities such as ITER.

IV.F. Induced Radioactivity Prediction

The irradiated materials included iron, nickel, chromium, Mn-Cu alloy, titanium, molybdenum, zirconium, tantalum, tungsten, silicon, magnesium, aluminum, vanadium, niobium, Type 316 stainless steel, tin, silver, lead, zinc, indium, and gold. The focus was on the gamma emitter radioisotopes with half-lives shorter than ~5 yr. The overall experimental error ranged from ±5 to ±15% in most cases. The sources of errors included counting statistics (error approximately ±5 to 10%), the gamma-ray detector efficiency (error approximately ±3%), and the neutron yield (error ±3%).

The details of the radioactivity experiments and calculations in the collaborative program are presented in Refs. 27 and 28. Calculations were conducted with several codes and libraries. The transport calculations were generally similar to those for tritium production, i.e., with the Monte Carlo and the discrete ordinates codes. The radioactivity calculations were performed using a number of available codes: ACT4 (Ref. 68), REAC (Ref. 69), RACC (Ref. 70), and DKR (Ref. 71). The cross-section and decay data libraries associated with these codes were used in addition to a number of new revised libraries in Japan and the United States. The sources of errors in the calculations are simulation of neutron spectra for neutron reactions with steep excitation functions around 14 MeV, which requires careful treatment for cross-section averaging; transport calculation of neutron flux, with the uncertainty estimated to be approximately ±20% for the (n,γ) reaction products; errors in the radioactivity code methodology, which were found to be generally small; and errors associated with radioactivity libraries (reaction cross sections and decay data).

Figure 28 shows typical C/E ratios for all materials considered with the focus on the gamma emitter radioisotopes with half-lives shorter than 5 yr. Most values for the C/E ratio range between 0.5 and 1.5, but some of them deviate greatly from 1 with some exceeding 5 and others falling below 0.1. Detailed analysis and identification of the sources of discrepancies are given in Refs. 27 and 28. The most common source of error found was physically unreasonable reaction cross-section values in the radioactivity libraries. Especially, several orders of magnitude differences were found in the cross sections for uncommon reactions, e.g., $(n,2p)$ and $(n,n'\alpha)$. Small values of C/E generally resulted from the lack of cross-section data for some important reactions in the radioactivity libraries. Figure 29 shows the C/E values for isotopic activities in Type 316 stainless steel. The deviation of C/E from 1 is particularly large for ^{57}Ni, ^{89}Zr, ^{99}Mo, ^{59}Fe, ^{57}Co, ^{58}Co, and ^{60}Co.

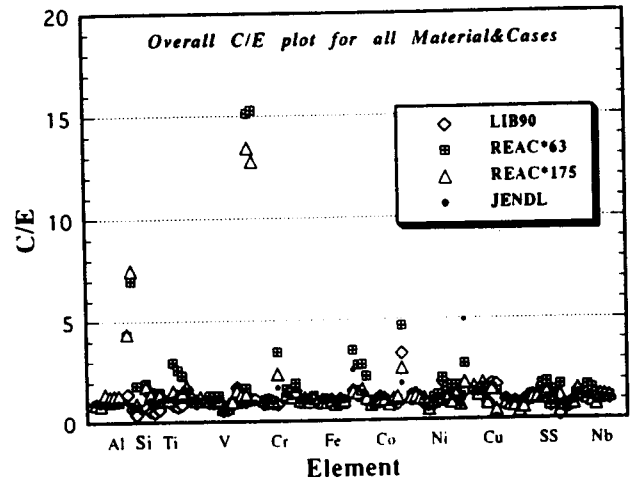

Fig. 28. Typical C/E ratios of decay radioactivity for the elements considered in the collaborative experiments. Decay radioactivity was measured for gamma emitter radioisotopes with half-lives shorter than 5 yr.

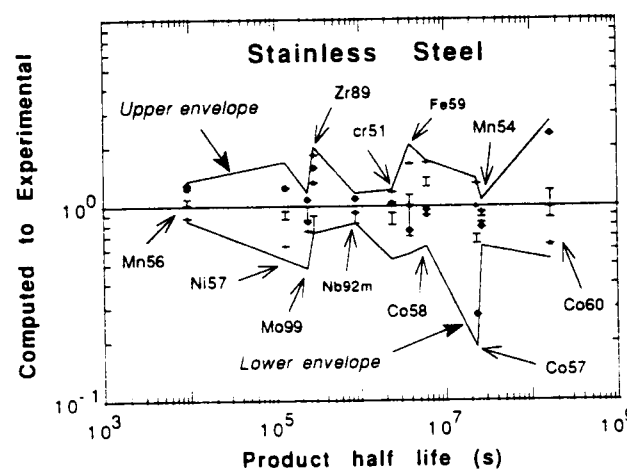

Fig. 29. Overall C/E values for isotopic activities in Type 316 stainless steel, using activation cross-section data contained in several libraries.

The overall conclusions from the radioactivity measurements are (a) there are large differences between calculations and experiments for a number of important materials; (b) in almost all cases for which C/E deviated from one, the source of error was attributed directly to inadequacies of activation libraries presently used with radioactivity codes; (c) the most common deficiency in activation libraries is errors in (or lack of) cross sections for certain reactions while other deficiencies include improper treatment of decay chains and erroneous data on product half-life, branching ratios, and decay gamma yields; and (d) there is a need to pursue further measurements, particularly for radioisotopes with long half-lives, but such measurements require a higher neutron yield and greater manpower.

IV.G. Total Nuclear Heating Prediction

As discussed earlier, the collaborative program succeeded in developing a microcalorimeter technique to measure the total nuclear heating using a 14-MeV neutron source. The measurements relied on measurements of a temperature rise in the probe material as small as 1 μK/s.

Measurements were made with a single-material probe for the following materials: carbon, aluminum, titanium, iron, nickel, copper, zirconium, niobium, molybdenum, tin, tungsten, and lead. Only the total nuclear heating was measured; i.e., the nuclear heating components of direct neutron heating and gamma-ray heating were not separated experimentally.

The details of the nuclear heating experiments and the calculations in the collaborative program are presented in Refs. 29 and 30. The neutron and gamma-ray transport calculations were carried out using the DOT 3.5 two-dimensional code and a three-dimensional representation in the MCNP Monte Carlo code. Different nuclear data libraries were used in the transport calculations, and they included RMCC (ENDF/B-V) and ENDL-85 with MCNP, and FUSION-J3 (JENDL-3) with DOT 3.5. The kerma factors used with the MCNP calculations came from the RMCC and ENDL-85 libraries. Some calculations also used kerma factors from the MATXS10 library based on ENDF/B-VI. Kerma factors were also generated from the JENDL-3 library.

Figure 30 gives an indication of the uncertainty in nuclear heating, expressed as C/E-1, for the various material probes subjected to D-T neutrons. Figure 30 shows results from ENDL-85, RMCC, MATXS10-heat, MATXS10-kerma, and JENDL-3, as well as a sensitivity estimate. Table V gives a summary of the C/E numerical values for nuclear heating in some single-probe materials.

The C/E value varies considerably from one material to another, and for a given material, it changes substantially from one library to another. The C/E deviates from unity by as much as 70% for some materials but by only a few percent for other materials.

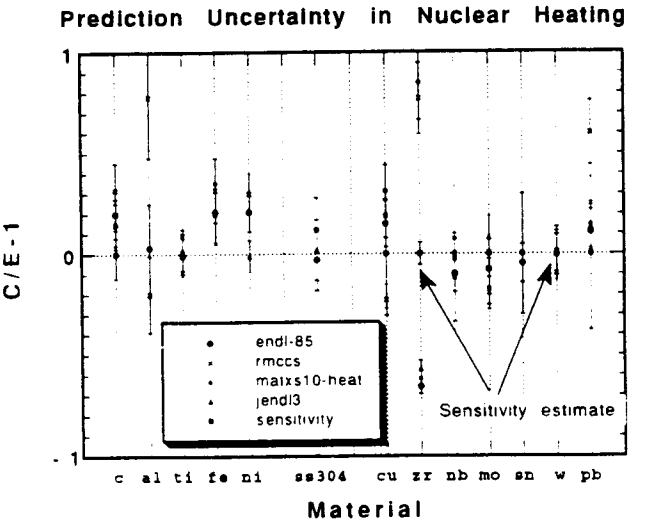

Fig. 30. Indication of uncertainty in nuclear heating, expressed as C/E-1, for various material probes subjected to D-T neutrons.

TABLE V

Summary of C/E Values for Nuclear Heating in Some Single-Probe Materials

Material	C/E		
	JENDL	RMCCS	ENDL-85
Aluminum	0.80 ± 0.19[a]	1.78	1.03
Titanium	0.99 ± 0.08	1.06	1.04
Iron	1.20 ± 0.15	1.32	1.21
Nickel	0.99 ± 0.08	1.3	1.21
Molybdenum	1.12 ± 0.06	0.84	0.96
Type 304 stainless steel	1.02 ± 0.15	1.12	0.97

[a]Experimental errors are considered. The same relative error should be associated with values for RMCCS and ENDL-85.

These large differences in predicting the total nuclear heating between experiments and calculations as well as among the different libraries is particularly alarming for two reasons. First, fusion reactor designs require an accuracy of the spatial distribution of nuclear heating of better than 10%. Nuclear heating rates, particularly in the first-wall/blanket regions, directly affect the temperature, which is a crucial parameter for determining thermal stresses, tritium inventories, radiation effects, and other phenomena related to steady-state performance and transient safety analysis. A 10% change in nuclear heating may result in a much larger effect in predicting these phenomena. Second, lower temperature limits are often as important as high-temperature limits. For example, there is a higher temperature limit for

operating structural materials. On the other hand, solid breeders have a temperature operating window with the upper limit determined by sintering and/or mass transport, while the minimum operating temperature is dictated by tritium diffusion. Therefore, the use of safety factors for nuclear heating is problematic. The design parameter space for fusion blankets is normally narrow and may not permit the use of two safety factors, one for the minimum and the other for the maximum temperature.

Therefore, the achievement of the collaborative program in performing the first measurements of the total nuclear heating with D-T neutrons must serve as a starting, rather than an end, point for a more substantive effort on measurements of nuclear heating. To date, the neutron and gamma heating components could not be separated during the integral measurements. Developing techniques that allow such separation can be a great step toward identifying the sources of error and an approach to improving nuclear heating calculations.

V. SUMMARY

A large number of integral experiments for fusion neutronics were carried out over a period of ~10 yr starting in 1984 as part of a JAERI/U.S. collaborative program. All experiments were conducted at the FNS facility at JAERI, which uses an accelerator-based D-T neutron source with a yield up to $\sim 3 \times 10^{12}$ n/s. The experiments focused initially only on tritium production and spectrum measurements in simplified prototypical blanket module assemblies. Later, a series of measurements for induced radioactivity and nuclear heating was carried out between 1989 and 1993 in addition to the tritium production and spectrum measurements.

The program of experiments proceeded in three phases: I, II, and III. In Phase-I, a cylindrical blanket test assembly, 60 cm in diameter and 61 cm in length and constructed of Li_2O blocks, was irradiated in open geometry. The front face of the test assembly received neutrons directly from the D-T source as well as neutrons scattered off the target room walls. In Phase-II, the test assembly and the source were surrounded by a rectangular enclosure of Li_2CO_3. This enclosure provided for a closed geometry in which room-returned neutrons were isolated, and the neutron spectra inside the enclosure simulated well those inside the plasma chamber of a fusion reactor. A number of experimental assemblies were used to examine the effects of beryllium, steel, and coolant-channel heterogeneities.

In Phase-III, a series of experiments was conducted using annular blanket test assemblies and a pseudo-line source geometry. This is quite different from Phases-I and -II, which used a point source geometry. The line-source geometry allowed better simulation of the spatial and angular flux distributions of D-T neutrons incident on the first wall of an MFE system.

One of the most important contributions of the collaborative program is the development of good measurement techniques to meet the specific requirements of fusion neutronics experiments. For tritium production measurements, several techniques were used. These included passive methods (Li-foil, Li_2O pellet, Li_2O-zonal, LiF-TLD) and active on-line methods (NE-213 and Li-glass). The experimental error associated with Li-foil and Li_2O-pellet was ~5%. Lower experimental errors are obtainable with the zonal method, but the detailed spatial resolution is lost.

The best present measurement techniques are limited in accuracy with ~3 to 5% error for tritium production, 5 to 10% for neutron spectrum, 3 to 6% for activation reactions, and 10 to 20% for gamma-ray heating rates. These limitations on the accuracy of measurement techniques represent one of the factors that must be accounted for in the design margin. Also note that most of the present measurement techniques cannot be applied in fusion devices where high temperatures and magnetic fields exist. Therefore, new measurement techniques should be developed for neutronics measurements in near-term fusion devices such as ITER.

Extensive measurements and calculations were performed for the spatial distribution of TPRs in ^6Li and ^7Li. State-of-the-art Monte Carlo and discrete ordinates codes with the most recent nuclear data libraries from ENDF/B in the United States and JENDL in Japan were used for the calculations. In general, the ratio of C/E was >1 by ~5 to 15%. However, there were cases, particularly in Phase-I, where the C/E values had much larger deviation from unity.

There were significant differences among measurement techniques and among calculational methods in predicting TPRs. A serious effort was devoted to quantifying the prediction uncertainty as well as safety factors for use in designs. To assure a 90% confidence level for line-integrated tritium production calculations not to exceed measurements, a safety factor of ~1.1 to 1.2, depending on the calculation method, should be used. These safety factors are derived based on the experiments in Phases-I, -II, and -III, which have much simpler blanket assemblies than those in an actual fusion reactor. Therefore, larger safety factors will be necessary to compensate for uncertainties in the complex, highly heterogeneous blankets in actual fusion reactors.

These safety factors may not be affordable in most present candidate blanket designs, which now barely meet the tritium self-sufficiency conditions. Therefore, we recommended that R&D related to all aspects of tritium breeding, extraction, processing, and fueling receive a high priority and that actual demonstration of tritium self-sufficiency be a high priority for testing in near-term fusion facilities such as ITER.

The fusion-like neutron spectra in the collaborative integral experiments provided a unique opportunity to perform reliable measurements of induced radioactivity in a number of materials. The technique of integral

measurements is very powerful as it can provide direct validation of radioactivity codes and data for a single isotope, an element, or an alloy with actual impurities. However, because of limitations on the neutron source yield and the human effort, only ~25 of materials were irradiated, and the focus was on the gamma emitter radioisotopes with a half-lives shorter than ~5 yr. The overall experimental error ranged from ±5 to ±15% in most cases. Calculations were conducted with all widely used radioactivity codes and libraries. Most values for the C/E ratio range between 0.5 and 1.5, but some of them deviate greatly from one with some cases exceeding 5 and others falling below 0.1.

The overall conclusions from the radioactivity measurements are as follows:

1. There are large differences between calculations and experiments for a number of important materials.

2. In almost all the cases for which C/E deviated from 1, the source of error was attributed directly to inadequacies of the activation libraries presently available with the widely used radioactivity codes.

3. The most common deficiencies in activation libraries are errors in (or lack of) cross sections for certain reactions; other deficiencies include improper treatment of decay chains, and erroneous data on product half-life, branching ratios, and decay-gamma yields.

4. There is a need to pursue further measurements, particularly for radioisotopes with longer half-lives, but such measurements require a higher neutron yield and greater manpower.

Because the theory and algorithm for nuclear heating calculations were developed ~25 yr ago, no measurements of the total nuclear heating with D-T neutrons had been carried out before the collaborative program started. The collaborative program attempted to perform such measurements. However, because of the relatively low neutron yield, only specialized experiments with small single-material probes were conducted. The microcalorimetric technique was vastly improved, and it allowed measurements of the total nuclear heating at FNS with a temperature rise as low as 1 μK/s.

The C/E value for the total nuclear heating is found to vary considerably from one material to another, and for a given material, there are large variations in the C/E derived from different kerma factor and transport libraries. The C/E ratio deviates from unity by as much as 70% for some materials but by only a few percent for others. These large discrepancies are alarming because the accuracy requirement on the spatial distribution of nuclear heating is better than 10%. Nuclear heating directly affects temperature. Many steady-state and transient performance phenomena in fusion nuclear components are very sensitive to temperature. Furthermore, there are generally lower as well as upper temperature limits, which makes the use of a single safety factor problematic. Therefore, the significant achievement of the collaborative program in performing the first measurements of nuclear heating with D-T neutrons must serve as a starting, rather than an end, point for a more substantive effort on measurements of nuclear heating.

The JAERI/U.S. collaborative program on fusion neutronics has made important contributions to identifying deficiencies in and suggesting improvements to codes and data for tritium breeding, nuclear heating, and induced radioactivity. As pointed out earlier, much more R&D is still needed. However, further progress will require a much larger investment in facilities and manpower. Also note that some important issues of fusion neutronics were not covered in the collaborative program, such as radiation shielding, radiation streaming, and biological dose inside and outside the reactor building. Some effort on shielding experiments is under way as part of the present R&D activities for ITER.

This paper focused on the technical achievements of the experiments and analyses of the collaborative program. One should note that the relatively long collaborative program has also demonstrated the many benefits of international cooperation. Finally, all participants from the United States and Japan feel that the "human experiment" of the collaborative program has enriched their lifetime experiences.

ACKNOWLEDGMENTS

The JAERI/U.S. collaborative program on fusion blanket neutronics greatly benefited from the support of the JAERI management and the Office of Fusion Energy (OFE) in the U.S. Department of Energy. The U.S. authors would like to express special thanks to S. Berk from OFE for continued support, encouragement, and helpful suggestions.

The authors acknowledge the untiring efforts made by the FNS operations staff. Thanks are also due the many scientists from various organizations in the United States and Japan who participated in some aspects of the work and/or provided useful advice.

We appreciate the skillful efforts of R. Holmes in preparing this manuscript.

REFERENCES

1. E. BERTOLINI, "Impact of JET Experimental Results and Engineering Development on the Definition of the ITER Concept," *Fusion Eng. Des.*, **27**, 27 (1995).

2. D. MEADE, "TFTR Experience with DT Operation," *Fusion Eng. Des.*, **27**, 17 (1995).

3. P. H. REBUT, "Detail of ITER Outline Design," *Fusion Eng. Des.*, **28** (1995).

4. T. NAKAMURA et al., "Fusion Neutron Source (FNS)," *Proc. 3rd Symp. Accelerator Science and Technology*, Osaka, Japan, August 27-29, p. 55, Osaka University (1980).

5. T. NAKAMURA and M. A. ABDOU, "Summary of Recent Results from the JAERI/U.S. Fusion Neutronics Phase I Experiments," *Fusion Technol.*, **10**, 541 (1986).

6. M. NAKAGAWA, T. MORI, K. KOSAKO, et al., "JAERI/US Collaborative Program on Fusion Neutronics—Phase-I Fusion Integral Experiments, Analysis," JAERI-M 88-177, Japan Atomic Energy Research Institute (1988); UCLA-ENG-88-15, University of California at Los Angeles (1988).

7. Y. OYAMA et al., "Phase-IIA and -IIB Experiments of JAERI/USDOE Collaborative Program on Fusion Blanket Neutronics," JAERI-M 89-154, Japan Atomic Energy Research Institute (1989).

8. M. NAKAGAWA, T. MORI, K. KOSAKO, Y. OYAMA, and T. NAKAMURA, "JAERI/USDOE Collaborative Program on Fusion Blanket Neutronics—Analysis of Phase-IIA and -IIB Experiments," JAERI-M 89-154, Japan Atomic Energy Research Institute (1989).

9. M. Z. YOUSSEF, M. A. ABDOU, Y. WATANABE, and P. M. SONG, "US/JAERI Collaborative Program on Fusion Neutronics—Phase-IIA and -IIB Fusion Integral Experiments, the US Analysis," UCLA-ENG-90-14 FNT-31, University of California at Los Angeles (1989).

10. Y. OYAMA et al., "Measured Characteristics of Be Multi-Layered and Coolant Channel Blankets: Phase IIC Experiments of the JAERI/USDOE Collaborative Program on Fusion Neutronics," *Fusion Technol.*, **19**, 1955 (1991).

11. M. Z. YOUSSEF, A. KUMAR, M. ABDOU, M. NAKAGAWA, K. KOSAKO, Y. OYAMA, and T. NAKAMURA, "Analysis for Heterogeneous Blankets and Comparison to Measurements: Phase IIC Experiments of the USDOE/JAERI Collaborative Program on Fusion Neutronics," *Fusion Technol.*, **19**, 1891 (1991).

12. T. NAKAMURA et al., "A Line D-T Neutron Source Facility for Annular Blanket Experiment: Phase III of the JAERI/USDOE Collaborative Program on Fusion Neutronics," *Fusion Technol.*, **19**, 1873 (1991).

13. C. KONNO et al., "Measurements of the Source Term for Annular Blanket Experiment with a Line Source: Phase IIIA of JAERI/USDOE Collaborative Program on Fusion Neutronics," *Fusion Technol.*, **19**, 1885 (1991).

14. H. MAEKAWA and M. A. ABDOU, "Overview of Latest Experiments under the JAERI/USDOE Collaborative Program on Fusion Neutronics," *Fus. Eng. Des.*, **18**, 275 (1991).

15. Y. IKEDA et al., "Measurement and Analysis of Nuclear Heat Depositions in Structural Materials Induced by D-T Neutrons," *Fusion Technol.*, **21**, 2190 (1992).

16. A. KUMAR, M. YOUSSEF, Y. IKEDA, C. KONNO, and Y. OYAMA, "Experiments and Analysis for Measurements of Decay Heat Related Induced Activities in Simulated Line Source Driven D-T Neutron Fields of Phase IIIA: USDOE/JAERI Collaborative Program on Fusion Neutronics," *Fusion Technol.*, **19**, 1859 (1991).

17. Y. IKEDA, C. KONNO, Y. OYAMA, T. NAKAMURA, A. KUMAR, M. Z. YOUSSEF, and M. A. ABDOU, "Experimental Verification of Current Data and Methods for Induced Radioactivity and Decay Heat Calculation in D-T Fusion Reactors," *Fus. Eng. Des.*, **18**, 387 (1991).

18. Y. IKEDA and M. Z. YOUSSEF, "Two-Dimensional Cross-Section Sensitivity and Uncertainty Analysis for Tritium Production Rate in Fusion-Oriented Integral Experiments," *Fusion Technol.*, **13**, 616 (1988).

19. Y. OYAMA, K. TSUDA, S. YAMAGUCHI, Y. IKEDA, C. KONNO, H. MAEKAWA, and T. NAKAMURA, "Phase II Experimental Results of JAERI/USDOE Collaborative Program on Fusion Blanket Neutronics Experiments," *Fus. Eng. Des.*, **9**, 309 (1989).

20. M. Z. YOUSSEF, Y. WATANABE, M. A. ABDOU, M. NAKAGAWA, T. MORI, K. KOSAKO, and T. NAKAMURA, "Comparative Analysis for Phase IIA and IIB Experiments of the U.S./JAERI Collaborative Program on Fusion Blanket Neutronics," *Fusion Technol.*, **15**, 1299 (1989).

21. Y. OYAMA et al., "Phase-IIC Experiments of the USDOE/JAERI Collaborative Program on Fusion Blanket Neutronics—Experiments and Analysis of the Heterogeneous Fusion Blankets, Volume I: Experimental Results," JAERI-M-92-182, Japan Atomic Energy Research Institute (Dec. 1992); see also UCLA-FNT-63, UCLA-ENG-93-18, University of California at Los Angeles (Dec. 1992).

22. M. Z. YOUSSEF et al., "Phase-IIC Experiments of the USDOE/JAERI Collaborative Program on Fusion Blanket Neutronics-Experiments and Analysis of the Heterogeneous Fusion Blankets, Volume II: Analysis," UCLA-FNT-64, UCLA-ENG-93-19, University of California at Los Angeles (Dec. 1992); see also M. NAKAGAWA et al., JAERI-M-92-183, Japan Atomic Energy Research Institute (Dec. 1992).

23. M. Z. YOUSSEF, Y. WATANABE, A. KUMAR, Y. OYAMA, and K. KOSAKO, "Analysis for the Simulation of a Line Source by a 14 MeV Moving Point Source and Impact on Blanket Characteristics: The USDOE/JAERI Collaborative Program on Fusion Neutronics," *Fusion Technol.*, **19**, 1843 (1991).

24. Y. OYAMA et al., "Phase III Experimental Results of JAERI/USDOE Collaborative Program on Fusion Neutronics," *Fus. Eng. Des.*, **18**, 203 (1991).

25. M. NAKAGAWA et al., "Characteristics of a Deuterium-Tritium Fusion Source on Rotating Target Used in Simulated Fusion Blanket Experiments," *Fusion Technol.*, **28**, 39 (1995).

26. Y. OYAMA et al., "Design and Techniques for Fusion Blanket Neutronics Experiments Using an Accelerator-Based

Deuterium-Tritium Neutron Source," *Fusion Technol.*, **28**, 56 (1995).

27. Y. IKEDA et al., "Measurements and Analyses of Decay Radioactivity Induced in Simulated Deuterium-Tritium Neutron Environments for Fusion Reactor Structural Materials," *Fusion Technol.*, **28**, 74 (1995).

28. A. KUMAR et al., "Decay Radioactivity Induced in Plasma-Facing Materials by Deuterium-Tritium Neutrons," *Fusion Technol.*, **28**, 99 (1995).

29. Y. IKEDA et al., "Direct Nuclear Heating Measurements and Analyses for Structural Materials Induced by Deuterium-Tritium Neutrons," *Fusion Technol.*, **28**, 156 (1995).

30. A. KUMAR et al., "Direct Nuclear Heating Measurements and Analyses for Plasma-Facing Materials," *Fusion Technol.*, **28**, 173 (1995).

31. Y. OYAMA et al., "Neutronics Integral Experiments of Lithium-Oxide Fusion Blanket with Heterogeneous Configurations Using D-T Neutrons," *Fusion Technol.*, **28**, 216 (1995).

32. M. YOUSSEF et al., "Nuclear Analysis of Integral Experiments on a Li_2O Test Assembly with Local Heterogeneities Utilizing a 14-MeV Neutron Source," *Fusion Technol.*, **28**, 243 (1995) (in press).

33. C. KONNO et al., "Neutronics Integral Experiments of Simulated Fusion Reactor Blanket with Various Beryllium Configurations Using Deuterium-Tritium Neutrons," *Fusion Technol.*, **28**, 273 (1995) (in press).

34. H. MAEKAWA et al., "A Summary of Benchmark Experiments for Simulation of Fusion Reactors Using an Annular Blanket with a Line Deuterium-Tritium Source," *Fusion Technol.*, **28**, 296 (1995) (in press).

35. Y. OYAMA et al., "Concept and Characteristics of a Simulated Line Source for Annular Blanket Experiments Using an Accelerator-Based Deuterium-Tritium Neutron Source," *Fusion Technol.*, **28**, 305 (1995) (in press).

36. M. YOUSSEF et al., "The Nuclear Analysis of an Annular Li_2O Blanket System Surrounding an Artificially Simulated 14-MeV Line Source and Comparison of Calculations to Measurements," *Fusion Technol.*, **28**, 320 (1995) (in press).

37. C. KONNO et al., "Neutronics Integral Experiments of Annular Blanket System Simulating Tokamak Reactor Configuration," *Fusion Technol.*, **28**, 347 (1995) (in press).

38. M. YOUSSEF et al., "Fusion Integral Experiments and Analysis and the Determination of Design Safety Factors—I: Methodology," *Fusion Technol.*, **28**, 366 (1995) (in press).

39. M. YOUSSEF et al., "Fusion Integral Experiments and Analysis and the Determination of Design Safety Factors—II: Application to the Prediction Uncertainty of Tritium Production Rate from the U.S. DOE/JAERI Collaborative Program on Fusion Blanket Neutronics," *Fusion Technol.*, **28**, 388 (1995) (in press).

40. M. A. ABDOU, "Radiation Considerations for Superconducting Fusion Magnets," *J. Nucl. Mater.*, **72**, 147 (Mar. 1978).

41. M. A. ABDOU, "Nuclear Design of the Blanket/Shield System for a Tokamak Experimental Power Reactor," *Nucl. Technol.*, **39**, 7 (1976).

42. J. JUNG and M. A. ABDOU, "Radiation Shielding of Major Penetrations in Tokamak Reactors," *Nucl. Technol.*, **41**, 71 (1978).

43. M. A. ABDOU et al., "Multidimensional Neutronics Analysis of Major Penetrations in Tokamaks," *Proc. 2nd Topl. Mtg. Technology of Controlled Nuclear Fusion*, Richland, Washington, September 21-23, American Nuclear Society (1976).

44. M. A. ABDOU et al., "Shielding and Maintainability in Experimental Tokamak," *Proc. 8th Symp. Engineering Problems of Fusion Research*, San Francisco, California, November 13-16, p. 645 (1979).

45. M. A. ABDOU et al., "Critical Technical Issues and Evaluation and Comparison Studies for Inertial Fusion Energy Reactors," *Fus. Eng. Des.*, **23**, 251 (1993).

46. LOS ALAMOS MONTE CARLO GROUP, "MCNP—A General Monte Carlo Code for Neutron and Photon Transport, Version 3A," LA-7396, Rev. 2, Los Alamos National Laboratory (1986).

47. M. NAKAGAWA and T. MORI, "Morse—DD, A Monte Carlo Code Using Multigroup Double Differential Form Cross-Sections," JAERI-M84-126, Japan Atomic Energy Research Institute (July 1984).

48. T. MORI, M. NAKAGAWA, and M. SASAKI, "Vectorization of Continuous Energy Monte Carlo Method for Neutron Transport Calculation," *J. Nucl. Sci. Technol.*, **29**, 325 (Apr. 1992).

49. J. C. NIMAL et al., "TRIPOLI-2 Programme de Monte Carlo Polycinétique à trois dimensions," Tomes I, II, III, DEMT/86/239, SERMA/LEPF/86/789, DEMT/86/240, SERMA/LEPS/86/799, Commissariat à l'Energie Atomique.

50. W. A. RHOADES and R. L. CHILDS, "An Updated Version of the DOT 4 (Version 4.3) One-and-Two-Dimensional Neutron/Photon Transport Code," ORNL-5851, Oak Ridge National Laboratory (Apr. 1982); see also CCC-429, Radiation Shielding Information Center, RSIC (1982).

51. W. A. RHOADES and R. L. CHILDS "The DORT Two-Dimensional Discrete Ordinates Transport Code," *Nucl. Sci. Eng.*, **99**, 88 (May 1988); see also CCC-484, Radiation Shielding Information Center (1988).

52. R. E. ALCOUFFE et al., "User's Guide for TWODANT: A Code Package for Two-Dimensional, Diffusion-Accelerated, Neutral-Particle Transport," LA-10049-M, Rev. 1.3, Los Alamos National Laboratory (1986).

53. T. MORI, M. NAKAGAWA, and M. SASAKI, "One-, Two-, and Three-Dimensional Transport Codes Using Multi-Group Double-Differential Form Cross Sections," JAERI-1314, Japan Atomic Energy Research Institute (Nov. 1988).

54. G. PALMIOTTI and M. SALVATORES, "Optimized Two Dimensional Sn Transport (BISTRO)," presented at Int. Topl. Mtg. Advances in Reactor Physics, Paris, France, April 27-30, 1987.

55. "ENDF-201, ENDF/B-VI Summary Documentation," BNL-NCS-17541 [ENDF-201], 4th ed., P. F. ROSE, Ed., Brookhaven National Laboratory (Oct. 1991).

56. K. SHIBATA et al., "JENDL-3," JAERI-1319, Japan Atomic Energy Research Institute (1990).

57. S. GANESAN and D. W. MUIR, "FENDL Multigroup Libraries," IAEA-NDS-129, International Atomic Energy Agency (July 1992).

58. M. A. ABDOU and C. W. MAYNARD, "Calculational Methods for Nuclear Heating—Part I: Theoretical and Computational Algorithms," *Nucl. Sci. Eng.*, **56**, 360 (1975).

59. M. A. ABDOU and C. W. MAYNARD, "Calculational Methods for Nuclear Heating—Part II: Applications to Fusion-Reactor Blankets and Shields," *Nucl. Sci. Eng.*, **56**, 381 (1975).

60. I. JUN, M. A. ABDOU, and A. KUMAR, "Impact of Ad Hoc Improvement of Decay and Cross Section Data on the Prediction of Fusion-Neutron Induced Radioactivity in Zirconium and Tungsten," *Fusion Technol.*, **25**, 51 (1994).

61. M. A. ABDOU and C. W. MAYNARD, "Neutronics and Photonics for CTR Blankets and Shields," FDM67, University of Wisconsin (July 1973).

62. M. A. ABDOU and C. W. MAYNARD, "Neutron Source Geometry Effects on Fusion Reactor Blankets," *Trans. Am. Nucl. Soc.*, **15**, 34 (1972).

63. S. MALANG et al., "Dual Blanket Concept," KfK 5424, Kernforschungszentrum Karlsruhe (Nov. 1994).

64. L. GIANCARLI et al., "Water-Cooled Pb-17 Li DEMO Blanket Line EU Reference Conceptual Design and Performance Presentation," DMT 94/538 (SERMA/LCA/1678), Commissariat à l'Energie Atomique (Dec. 1994).

65. M. DALLE DONNE et al., "BOT Solid Breeder Blanket," KfK 5429, Kernforschungszentrum Karlsruhe (Nov. 1994).

66. M. EID et al., Ed., "Helium-Cooled Ceramic-Breeder-in-Tube Blanket Line," Report RI-RCT 9412, Commissariat à l'Energie Atomique and ENEA (1994).

67. M. A. ABDOU, E. L. VOLD, C. Y. GUNG, M. Z. YOUSSEF, and K. SHIN, "Deuterium-Tritium Fuel Self-Sufficiency in Fusion Reactors," *Fusion Technol.*, **9**, 250 (1986).

68. Y. SEKI et al., "THIDA-2: An Advanced Code System for Calculation of Transmutation, Activation, Decay Heat, and Dose Rate," CCC-410, Radiation Shielding Information Center Computer Collection (Apr. 1987).

69. F. H. MANN, "REAC*2: Users' Manual and Code Description," WHC-EP-0282, Westinghouse Hanford Company (1989).

70. J. JUNG, "Theory and Use of Radioactivity Code RACC," ANL/FPP/TM-122, Argonne National Laboratory (May 1979).

71. D. L. HENDERSON and O. YASAR, "A Radioactivity and Dose Rate Calculation Code Package," CCC-323, Radiation Shielding Information Center Computer Code Collection (Apr. 1987).

Mohamed A. Abdou is a professor in the Department of Mechanical, Aerospace, and Nuclear Engineering at the University of California, Los Angeles (UCLA) and also is the director of fusion technology at UCLA. His research interests include neutronics, thermomechanics, fusion technology, and reactor design and analysis. He served as the U.S. leader of the Japan Atomic Energy Research Institute (JAERI)/U.S. Department of Energy (U.S. DOE) collaboration on fusion blanket neutronics.

Hiroshi Maekawa (BE, 1965; MS, 1967; and Dr. Eng., 1970, nuclear engineering, Tokyo Institute of Technology, Japan) is the deputy director of the Department of Reactor Engineering and the head of the Intense Neutron Source Laboratory at JAERI. He has worked on fusion neutronics for more than 20 years, and he planned and constructed the Fusion Neutronics Source (FNS) facility. He served as the Japanese leader of the JAERI/U.S. DOE collaboration on fusion blanket neutronics. His recent research has focused on International Fusion Materials Irradiation Facility conceptual design activities.

Yukio Oyama (BS, physics, 1975; MS, nuclear physics, 1977; and Dr. Eng., 1989, Osaka University, Japan) is a principal scientist at JAERI. He has worked in the area of fusion neutronics experiments since 1978. He is currently involved in intense and high-energy neutron source projects.

Mahmoud Z. Youssef (PhD, nuclear engineering, University of Wisconsin, 1980) is a senior research engineer in the Department of Mechanical, Aerospace, and Nuclear Engineering at UCLA. He participated in several conceptual magnetic fusion energy and inertial fusion energy reactor design studies with emphasis on nuclear analysis and blanket/shield design. His research interests are in the areas of blanket/shield design optimization, nuclear data, sensitivity/uncertainty studies, neutronics methods and code development, tritium fuel cycle, radioactivity and safety aspects of fusion, integral experiments, neutronics testing, and research and development for fusion reactors, particularly the International Thermonuclear Experimental Reactor (ITER).

Yujiro Ikeda (PhD, nuclear engineering, Nagoya University, Japan, 1981) is head of the Fusion Neutronics Laboratory in the Department of Reactor Engineering at JAERI. He has worked in the areas of fusion neutronics experiments, induced radioactivity experiment and analysis, direct nuclear heating measurements, activation cross-section measurements, and fusion dosimetry.

Anil Kumar (PhD, University of Bombay, India, 1981) is senior development engineer at UCLA. His current research interests include fusion reactor nucleonics experiments and analysis, technique development for nuclear heating, decay heat measurements, biological dose, fusion diagnostics, safety factor methodology for fusion reactor design parameters, low-activation materials, inertial confinement fusion, and sequential reactions. He has conducted experiments at leading facilities such as the FNS facility in Japan, the Tokamak Fusion Test Reactor (TFTR) at Princeton University, and LOTUS in Switzerland.

Chikara Konno (MS, physics, Kyoto University, Japan, 1985) is a research scientist in the Department of Reactor Engineering at JAERI. He has worked in the areas of fusion neutronics experiments, cross-section measurements, and neutron spectrum measurements using a proton-recoil counter.

Fujio Maekawa (MS, nuclear engineering, Osaka University, Japan, 1990) is a research scientist at JAERI. He has been engaged in integral experiments for fusion neutronics and studied the behavior of neutron, photon, and electron transport in media. His current interests are in the measurements of tritium and decay heat of irradiated materials.

Kazuaki Kosako (BE, atomic engineering, Tokai University, Japan, 1984) has worked at Sumitomo Atomic Energy Industries since 1994. He worked in the Department of Reactor Engineering at JAERI from 1984 to 1992 where he was involved mainly in fusion neutronics. He is currently interested in the area of radiation damage of materials.

Tomoo Nakamura (BS, physics, Kyoto University, Japan, 1957) is currently director of the Public Acceptance Database Center, Research Organization for Information Science and Technology. His research background includes experimental reactor physics on fast breeder reactors and nuclear technology on fusion reactor blankets. He served as the former Japanese leader of the JAERI/U.S. DOE collaboration on fusion blanket neutronics.

Edgar F. Bennett (PhD, University of New Hampshire, 1957) is a physicist at Argonne National Laboratory. He has been a section head of experimental reactor physics since 1970. He is best known as the inventor of a widely used in-core proton-recoil spectrometer—a technique that he has been continually updating. He has also made contributions to the field of reactivity measurement by reactor noise techniques, in particular, by providing a common theoretical basis and introducing a new type of variance experiment.